FRONT MATTER

Title

What do Functional Synchronization Networks Indicate About Underlying Structure and System Dynamics? A network theory study of the islet.

Short Title

Understanding Functional and Structural Networks

Authors

Jennifer K. Briggs[1], Vira Kravets[1,2], JaeAnn M. Dwulet[1], David J. Albers[1], Richard K. P. Benninger*[1,2]

1. Department of Bioengineering, University of Colorado Anschutz Medical Campus, Aurora, Colorado
2. Barbara Davis Center for Childhood Diabetes, University of Colorado Anschutz Medical Campus, Aurora, Colorado

* Corresponding author: richard.benninger@cuanschutz.edu

Abstract

Network theory provides tools for quantifying communication within heterogeneous biological systems. Functional and structural networks are common way to represent a biological system. The relationship between these two networks is not well quantified, leaving a knowledge gap for how to interpret functional networks in the context of structural changes. In diabetes, both structural and functional networks of the islet of Langerhans are altered, motivating the investigation as to how the two networks interact. Here, we analyze both experimental and computational models of the islet to quantify the relationship between the gap junction structural network and functional synchronization networks. We show that functional networks poorly reflect gap junction structure. Instead, they indicate intrinsic factors driving excitability, such as cellular metabolism. This surprising finding provides a new interpretation of functional networks within the islet of Langerhans and other biological systems.

Teaser

We use experimental and computational models to provide a new interpretation of intracellular synchronization in biological networks.

MAIN TEXT

Introduction

Our understanding of biological systems has benefitted from the application of network theory *(1–4)*, a set of analysis techniques used to quantify the relationships between interacting parts of a system. In network analysis, a system is represented by its entities (called nodes) and the interactions between those entities (called edges). The topology and degree structure of the network **(Table 1)** can then provide information about the biological system.

To apply network theory tools, one must decide how to represent the system. Common network representations in biological tissues are based on either structure or function *(5–7)*. In both representations, nodes generally correspond to physical neurons, cells, or regions of interest. The difference between structure and function lies in how the edges are constructed. *Structural networks* represent physical connections between nodes; therefore, edges correspond to physical connections, such as synapses or gap junctions. However, in complex systems, such as most biological systems, the structure network alone cannot explain how the system works *(5)*. Instead, functional behavior emerges from complex interactions between individual cell dynamics and the underlying structure *(2, 8)*. *Therefore, functional networks* are meant to represent the emergent system behavior, where edges correspond to functionally similar cell pairs.

When deciding whether to use a functional or structural network, one must consider both the research question they are investigating and the tools accessible to them. A *structural network* preserves spatial information and should be used when asking questions concerning node influence through physical communication or a physical change in the system. Obtaining a complete structural network of a biological system requires imaging the entire 3D system with techniques that differentiate cells and cell connections. Such network reconstruction may be an impossible task for some systems *(7)* and is highly labor-intensive for others. *Functional networks* should be used when quantifying emergent system behavior. Functional networks are often generated by drawing edges between pairs of neurons or other cells that show highly correlated dynamics, for example, as observed through calcium-based imaging *(5, 8–10)*. Many network-informed biological studies utilize synchronization-based functional networks because calcium-based imaging approaches are relatively common *(9, 11, 12)* and more accessible than directly identifying structural connections. Since functional networks are more common and accessible than structural networks in biology, it is relatively common for scientists to draw conclusions about the systems' structure by using the structural network. This conclusion relies on the assumption that structure and function have a 1-to-1 correspondence, which may not always be the case. In this paper, we investigate the relationship between structural and functional networks to assess the validity of this assumption.

Considered independently, structural and functional networks can solve interesting questions regarding physical communication or emergent dynamics *(5)*. However, we are often concerned with the intersection between these concepts: such as how physical changes in the structural network relate to emergent dynamics in the functional network. Little is known about this interaction between functional and structural networks. One system in which this is critically important is the pancreatic islet, which is the focus of this paper. Pancreatic islets are comprised of insulin-producing, highly heterogeneous β-cells that electrically communicate through connexin36 (Cx36) gap junctions *(13–15)*. This communication allows for insulin release in coordinated pulses *(13, 16–18)*. Coordinated pulsatile

behavior is central to regulating the homeostasis of glucose and other nutrients *(19–21)* and is lost during the development of type 1 and type 2 diabetes *(20, 22)*. Loss of intra-islet coordination in diabetes is associated with changes in the *functional β-cell network*. However, it is unclear how disruption in the functional network is related to changes in individual β-cell function and disruptions in the structural network, as type 1 and some presentations of type 2 diabetes are also associated with dysfunction or death of insulin-producing β-cells and loss of gap junction coupling *(22–26)*. Therefore, understanding the interaction between structure, function, and system dynamics is important.

Studies have suggested that the functional β-cell network follows a scale-free-like distribution *(9)* with a tendency toward high clustering *(27, 28)*, implying there exists a subset of highly connected nodes called "β-cell hubs" *(6, 10)*. Note that mathematically scale free networks are rare in nature *(29)*, so we use the term scale-free-like to describe a distribution with a roughly logarithmic distribution. Since these hubs emerge from the functional network, it is unclear whether their high synchronization is due to physical influence via higher than average structural coupling or intrinsic properties of the β-cells themselves. Functional network studies suggest that these emergent β-cell hubs have a large influence over islet dynamics *(10, 30, 31)*. Alternatively, proxies for structural networks, such as electrophysiological experiments and computational studies measuring gap junction electrical coupling, suggest it is not feasible for one cell or a small population of cells to have disproportionate influence over the islet *(30, 32–34)*. These seemingly contradicting results have caused debate over the most accurate topological description of the islet network *(35, 36)* (see *(37)* for a concise review of the β-cell hub debate) and motivated our investigation of the relationship between structure and function of the islet.

In this paper, we use experimental and computational techniques to investigate the relationship between the structural and functional networks using three guiding questions (results are graphically outlined in **figure 8)**. 1) Are subpopulations that emerge from the β-cell functional network differentiated by a unique location in the structural network or by intrinsic properties of the cells? 2) What does the islet functional network indicate about its underlying structure or intrinsic cell properties? 3) Can we fully explain the disruption in the functional network by the removal of nodes and edges in the structural network, or are there other factors involved? Our data lead to the conclusion that the islet functional network is more reflective of variability in cellular metabolic activity than gap junction structural connections. These results provide fresh insight into interpreting the relationship between structure, function, and intrinsic cell dynamics in the pancreatic islet.

Results

Cellular metabolism is more influential than gap junction coupling in determining highly synchronized cells in a simulated β-cell network.

Accurately analyzing the structural network or the intrinsic factors underlying cellular excitability is non-trivial to perform experimentally. Thus, to investigate the relationships between functional and structural networks, we first analyzed a simulated β-cell network. We used a multi-cellular coupled ODE model, which describes the electrophysiological properties of the β-cells. This model has been shown to accurately describe experimental findings concerning spatial-temporal dynamics *(38)*, the relationship between electrical coupling and metabolic heterogeneity *(39)*, the relationship between electrical heterogeneity and electrical activity *(40)*, and the influence of excitability parameters such as rate of glucose metabolism (k_{glyc}) and K_{ATP} channel opening kinetics on diabetes mutations *(39, 41)*. Our model included physiologically informed heterogeneity in multiple factors underlying cellular excitability and in gap junction electrical coupling (**Figure 1a**).

The first question we investigated was: Are subpopulations that emerge from the β-cell functional network differentiated by a unique location in the structural network or by intrinsic properties of the cells? Specifically, we first investigated whether β-cell hubs are differentiated by a unique location in the structural network or by the inherent properties of the cell? We first created the simulated islet's functional network of the intracellular free Ca^{2+} ($[Ca^{2+}]$) dynamics. We represented each cell with a node and drew an edge between any cell pair whose temporal calcium traces had a Pearson correlation coefficient (R_{ij}) greater than the threshold R_{th}. In a network, the degree is defined as the number of edges a given cell has, while the degree distribution describes the distribution of degrees throughout the network **(Table 1).** We set the threshold to $R_{th} = 0.9995$, so the normalized degree distribution showed the presence of many cells with a relatively low degree and a few cells with a very high degree in the five simulated islets (**Figure 1b**), as indicated in previous studies *(9, 10)*. This power law-like distribution shows that the functional network acts as a scale-free-like distribution (Table 1), which implies that few cells in the islet are highly synchronized while most cells are not. One way to interpret a scale-free-like distribution is that highly synchronized cells are driving or coordinating the islet function.

We then identified a subpopulation of highly synchronized cells, referred to as β-cell hubs, as any cell whose degree (see **Table 1)** was greater than 60% of all other cells in the functional, as outlined in *(10)*. Within a simulated islet, multiple such β-cell hubs were present (**Figure 1c).** These β-cell hubs tended to depolarize before and repolarize after the islet average (**Figure 1d**), in agreement with previous studies *(10)*. We next analyzed the properties of these highly connected β-cell hubs. Johnston et al. showed that β-cell hubs have higher than average metabolic activity *(10, 41);* therefore, we chose to investigate this parameter. Critical factors which influence β-cell excitability include the rate of glucose metabolism to generate ATP (k_{glyc}) and the activity of ATP-sensitive K^+ (K_{ATP}) channels. β-cell hubs had a significantly higher rate of glucose metabolism (k_{glyc}) than non-hubs ($p \leq 0.0001$) (**Figure 1e**) but were not significantly different in their maximum K_{ATP} conductance (g_{KATP}) ($p = 0.18$) (**Figure 1f**). These results indicate that β-cell hubs are differentiated by glucose metabolism rather than K_{ATP}-dictated cellular excitability. Interestingly, β-cell hubs had only a slightly higher gap junction conductance (g_{coup}) than non-hubs ($p = 0.032$) **(Figure 1g).** To ensure consistency in our findings, we repeated the following analysis with various thresholds **(Supplemental 1a)**. For all thresholds analyzed,

148 the significance between hubs and non-hubs was greater for k_{glyc} than g_{coup} **(Supplemental 1b)**. These
149 results indicate that both metabolic activity and gap junction coupling correlate with high cellular
150 synchronization, where the rate of metabolic activity has a stronger correlation.

151 Elevated cellular metabolic activity, but not elevated gap junction permeability is observed
152 experimentally in highly connected cells

153 To further investigate question 1 concerning subpopulations that emerge from the β-cell functional
154 network, we tested whether the properties of highly connected cells that we identified within the
155 simulated network occur experimentally within islets of Langerhans. We performed time-lapse imaging
156 of [Ca^{2+}] within islets isolated from Mip-CreER; Rosa-LSL-GCamp6s mice that express GCamP6s
157 specifically in β-cells (β-GCamP6s mice, see methods). At elevated glucose, islet β-cells showed
158 synchronous oscillations in [Ca^{2+}] (**Figure 2a,b**). We performed Pearson-based functional network
159 analysis on these [Ca^{2+}] time-courses (see methods) (**Figure 2c)** and generated a normalized degree
160 distribution that describes this experimentally-derived functional network (**Figure 2d**), which again
161 reflects a large number of cells with low degree and few cells with high degree, which can be interpreted
162 as a scale-free-like distribution (Table 1).

163 To test whether cellular metabolic activity differentiated high-degree cells from normal or low-
164 degree cells in the functional network, we performed two-photon excitation of NAD(P)H
165 autofluorescence of β-cells in conjunction with time-lapse imaging of Ca^{2+} dynamics at 2- and 11-mM
166 glucose levels (**Figure 2e**). The metabolic activity of individual cells in the islet was calculated as a
167 difference between the NAD(P)H autofluorescence level at high glucose compared to low glucose
168 ($NAD(P)H_{11\text{-}2}$). This was adjusted by the mean change in autofluorescence across all cells in the islet
169 ($NAD(P)H_{11av\text{-}2av}$). Therefore, the metric was 0 if the NAD(P)H response of a cell was the similar to the
170 islet average, >0 if a cell showed an elevated metabolic response indicating it is more metabolically
171 active, and <0 if a cell showed a reduced metabolic response indicating it is less metabolically active.
172 The NAD(P)H response to glucose elevation decreased as the cell's normalized degree decreased
173 (**Figure 2f)**. This indicates that highly synchronized cells are more metabolically active, as measured by
174 NAD(P)H autofluorescence, in agreement with findings from simulated islets. Furthermore, the
175 NAD(P)H response trended lower in cells that were functionally disconnected, as indicated by Ca^{2+}
176 oscillations lacking synchronization with any other cells, compared to the NAD(P)H response in
177 connected cells **(Figure 2g)**. Therefore, the functional network is strongly related to metabolism which
178 drives islet dynamics.

179 While it is not possible to experimentally measure the strength of every gap junction connection
180 across the islet, fluorescence recovery after photobleaching (FRAP) measurements of dye transfer
181 kinetics can measure the gap junction permeability within the islet with cellular resolution *(43)*. We
182 performed FRAP measurements of gap junction permeability using a Cx36 gap-junction-permeable
183 tracer Rhodamine-123 in conjunction with Ca^{2+} time-lapse imaging of GCamP6s, to map cellular gap
184 junction connections in the same cell layer as functional connections are calculated (**Figure 2h,i**). We
185 found that the rate of recovery, which assesses gap junction permeability, lacked any trend with Ca^{2+}
186 synchronization such that cells with high degrees showed similar permeability as cells with low degrees
187 **(Figure 2j)**. This indicates that cell synchronization was not strongly correlated with gap junction

permeability, as measured by FRAP, which is consistent with findings from the simulated islet. Therefore, the functional network is not strongly related to the structural network.

<u>A synchronized cell pair is more likely to indicate shared metabolic properties between the cells than a shared gap junction.</u>

Our findings so far indicate that highly synchronized cells within the functional network correlate more strongly with intrinsic metabolic properties such as metabolic rate and activity than with gap junction electrical connections. We then investigated the second question: What does the islet functional network indicate about its underlying structure or intrinsic cell properties? We observed few instances in which a cell pair was connected in both the functional and structural networks (**Figure 3a**), irrespective of a cell's degree of synchronization (considering highly connected β-cell hubs, cells with average synchronization, or cells with low synchronization**).** This indicates that cellular synchronization does not imply the presence of a gap junction. To quantify this relationship, we calculated the conditional probabilities of finding edges in the functional and/or structural networks. The probability that two cells were synchronized in the functional network given that they shared a gap junction in the structural network, $Pr(Sync|GJ) = 0.39$ (**Figure 3b**). Therefore, less than half of cell pairs that are electrically coupled by gap junction connections are considered to be functionally coupled. The alternative probability of a structural edge given a functional edge, $Pr(GJ|Sync) = 0.04$ (**Figure 3b**), indicating that very few cells that are functionally coupled are directly connected by gap junction connections. These findings indicate cells that are connected in the structural network (gap junction) and cells that are connected in the functional network (synchronized [Ca^{2+}] dynamics) are two distinct groups with little overlap ($Pr(both) = 0.2$) (**Figure 3c**).

We again analyzed the sensitivity of these measures to synchronization threshold R_{th}. By nature of the method used to create the functional network, as the threshold was increased, the number of cells considered synchronized substantially decreased (**Supplemental 1d**). The probability that two cells were gap junction coupled given that they were connected in the functional network greatly increased with increasing correlation threshold (**Supplemental 1e**), such that when $R_{th} = 0.99995$, $\Pr(GJ|Sync) \approx 0.5$. This was not due to an increasing "overlap" between the functional network and structural network, but rather the decrease in the size of the functional network sample space (**Supplemental 1f**). Therefore, our findings that the functional and structural networks are two distinct groups with little overlap is consistent across thresholds.

These data corroborate with initial findings showing that function is not strongly correlated with structure. To investigate whether metabolic properties are correlated with function, as shown in our previous results, we created two new networks involving rate of glucose metabolism (k_{glyc}). In the first network (i), we drew an edge between cells if they had similar rates of k_{glyc} and were separated by less than 15 cells (see methods) **(Figure 3d light green).** In the second network (ii), we drew an edge between cells if they had higher than average rates of k_{glyc} and were separated by less than 15 cells **(Figure 3d dark green).** We chose these parameters such that there was no difference in the probability of synchronization (edge in the functional network) given a gap junction or metabolic quality (**Figure 3e**). The alternative probability of unique properties in glucose metabolism (similar or high k_{glyc}) given a functional edge was significantly higher than that of structural connections ($p \approx 0.005$ for both networks **(Figure 3f)**. While total number of links was larger in the metabolic networks, it is unlikely that these

229 results were caused by a difference in sample size given the initial probabilities Pr $(Sync|GJ)$ and
230 Pr $(Sync|k_{glyc})$ were similar. Therefore, if two cells have synchronized Ca^{2+} oscillations, they are more
231 likely to show either similar metabolic activity or have higher than average metabolic activity, compared
232 to the two cells that are gap junction coupled. This is further indicated by the increased overlap between
233 the Ca^{2+} synchronization-derived functional network and the metabolic activity-derived network (**Figure**
234 **3g**). These results further indicate that metabolic activity, not gap junction connections, is a greater
235 driving factor for cells to show high Ca^{2+} synchronization and thus influence the functional network, in
236 agreement with our previous findings.

237 Elevated cellular rate of glucose metabolism is a greater driver of long-range functional connections.
238 We noted that in the simulated islet model, gap junction connections only exist between highly proximal
239 cells, in accordance with the islet cytoarchitecture. However, there was no distance constraint on $[Ca^{2+}]$
240 oscillation synchronization (**Figure 4a**). To determine whether this spatial constraint was responsible
241 for the low correspondence between the functional and structural networks, we asked whether a series
242 of highly conductive gap junction connections could predict long-range functional connections. Previous
243 work has shown that that long-range functional connections can arise without assuming long-range
244 structural connections *(44)*. We can assess the total gap junction conductance along a path connecting
245 two cells by weighting the structural network by gap junction conductance. We then calculated the path
246 which maximized conductance between every cell pair in the simulated islets (**Figure 4b**) (see methods:
247 shortest weighted path length), allowing us to quantify the chains of highly conductive gap junctions.
248 We then partitioned the cell pairs based on whether or not they were connected in the functional network.
249 We express our results as the total g_{coup} for different distances of cell separation. In some cases, the total
250 g_{coup} between a given cell and a cell it was synchronized with was greater than that between the given
251 cell and a non-synchronized cell of the same cell distance, **(Figure 4b top)** while in other cases the non-
252 synchronized cell showed a higher total g_{coup} **(Figure 4b bottom).** This indicates that not all
253 synchronized cell pairs have higher chains of gap junction conductance than non-synchronized cell pairs.
254 Further, the probability distributions of total conductance for synchronized cells highly overlapped with
255 those for non-synchronized cells. This was observed for cells that were directly gap junction coupled
256 (**Figure 4c**) and cells that showed longer-range functional connections (**Figure 4d**). We compared the
257 total conductance between all cells irrespective of separation distance by normalizing the total
258 conductance by separation distance. The normalized total conductance was slightly less for non-
259 synchronized cells than for synchronized cells (**Figure 4e**), although still with substantial overlap
260 (**Figure 4 c,d)**. Thus, long-range functional connections traverse cells that are connected on average by
261 slightly higher gap junction conductance. However, the substantial overlap in total conductance between
262 synchronized and non-synchronized connections is consistent with the minor influence of gap junction
263 conductance in driving high synchronization between cells. Therefore, while gap junction conductance
264 influences long-range synchronization, it is not the driving factor and cannot be used to differentiate cell
265 pairs connected in the functional network.
266 To examine how cellular rate of glucose metabolism influenced long-range functional
267 connections, we repeated this procedure but weighted graph edges by k_{glyc} rather than coupling
268 conductance (g_{coup}). Weighting the network edges by k_{glyc} allows us to quantify whether highly
269 synchronized cells result from chains of cells with high rates of glucose metabolism. We present the total

k_{glyc} along the path which maximized k_{glyc} between two cell pairs for different distances of cell separation. Again, the probability distributions of the total k_{glyc} for synchronized cells were highly overlapping with that for non-synchronized cells; both for cells that were directly gap junction coupled (**Figure 4f**) and cells that showed longer-range functional connections (**Figure 4g**). The total rate of glucose metabolism, normalized by separation distance, was significantly less for non-synchronized cells than for synchronized cells (**Figure 4h**), with little overlap. Thus, long-range functional connections on average traverse cells with higher rates of glucose metabolism.

To test whether there was a spatial relationship for which rate of glucose metabolism or gap junction conductance-controlled synchronization, we then analyzed the total conductance or total cellular metabolic rate for different separation distances compared between synchronized cells or non-synchronized cells. Cumulative distribution functions (CDFs) reveal the small difference in total conductance (**Supplemental 1**) or total rate of glucose metabolism (**Supplemental 2**) for each cell separation distance. Synchronized cells had significantly higher total cellular metabolic rate than non-synchronized cells for distances 1 to 5 cells apart, with very high level of significance (see methods, significance testing). Conversely gap junction conductance was significantly higher for only synchronized cells 2, 4, 5, 6, and 7 distances apart, with a lower level of significance (average significant $\mathrm{P}_{\mathrm{k}_{\mathrm{glyc}}} = 0.0064$ and average significant $\mathrm{P}_{\mathrm{g}_{\mathrm{coup}}} = 0.0194$). Thus, cells pairs with similar metabolic rate can strongly influence longer-range function connections up to distances of 5 cells apart. In contrast, cells with higher gap junction conductance have less influence over longer-range functional connections. Nevertheless, gap junctions retain some influence over long distances.

<u>Individual gap junction connections cannot be predicted by the functional network with correlated gap junction conductance and metabolic activity.</u>

Our computational model assumes that metabolic parameters and gap junction coupling are independent. However, it has previously been suggested that cells with highly synchronized Ca^{2+} oscillations possess both elevated metabolic activity (in agreement with our findings, **Figure 2**) *and* high levels of gap junction conductance (unlike what we see in our experiment, **Figure 2**) *(10, 31)*. To address the possibility that cells with high metabolic activity may also have higher levels of gap junction conductance, we simulated an islet in which the rate of glucose metabolism positively correlated with gap junction conductance (**Figure 5a**), similar to the distribution presented in *(30)*, and generated the functional network (**Figure 5b**). There was no difference in the average degree of the functional network (i.e., average islet synchronization) between the random distribution (**Figure 1**) and this proportional distribution (**Figure 5c).** Highly synchronized β-cell hubs had a significantly higher metabolic rate compared to non-hubs (**Figure 5d**). In this simulated islet the gap junction conductance was also significantly higher in hubs (**Figure 5e**), as expected given that cells with higher k_{glyc} are programmed to have higher g_{coup}. Again, there was no significant difference in g_{KATP} between β-cell hubs and non-hubs (**Figure 5f**). As with a normal distribution, the probability that two cells were synchronized in the functional network given that they shared a gap junction connection in the structural network ($\Pr(Sync|GJ)$=.303) was much greater than the alternative probability of a structural edge given functional edge ($\Pr(GJ|Sync)$=0.027) (**Figure 5g)** Importantly, both $\Pr(Sync|GJ)$ and $\Pr(GJ|Sync)$ were smaller than the equivalent probabilities determined when k_{glyc} and g_{coup} are not correlated (**Figure 5g**, **Figure 3b**). Therefore, the structural network still could not be effectively derived from the

311 functional network **(Figure 5 g,h).** We calculated the total g_{coup} between synchronized and non-
312 synchronized cells along weighted networks using the previous methodology. The total g_{coup} was
313 significantly higher for cell distances from 1-9 and 14 cells apart **(Figure 5i)**. Therefore, when g_{coup} is
314 proportional to k_{glyc}, synchronization is more predictive of long-range connections mediated by high gap
315 junction conductance than of individual gap junction connections.

316 <u>Modulating the islet-wide structural network in Cx36 knockout islets</u>
317 Our final question was: Can we fully explain the disruption in the functional network by the removal of
318 nodes and edges in the structural network, or are there other factors involved? This question is
319 particularly relevant in pathophysiological conditions, where physical connections or cells are removed
320 from the system. Given that Cx36 forms gap junction channels that enable electrical communication
321 between β-cells, reducing or eliminating Cx36 will remove edges from the structural network. It is well
322 established that changes to gap junction conductance affect the emergent Ca^{2+} dynamics across the islet
323 *(13)*. We performed functional network analysis on time-courses of oscillatory [Ca^{2+}] dynamics in islets
324 from wild-type mice with standard gap junction coupling ($Cx36^{+/+}$), heterozygous Cx36 knockout mice
325 with approximately 50% reduced gap junction coupling ($Cx36^{+/-}$) and homozygous Cx36 knockout mice
326 with no gap junction coupling ($Cx36^{-/-}$) *(13)* (**Figure 6a-c**). To ensure consistency across genotypes, we
327 chose a synchronization threshold R_{th} such that the degree distribution of the WT islets was similar to a
328 scale-free-like distribution *(9)* while the average network degree ranged from 5-15 (see methods).
329 **Figure 6c** shows representative degree distributions of the functional networks corresponding to
330 the islets shown in **Figure 6a**. Average histograms of the degree distribution for all islets are presented
331 in **Supplemental 4a**. Results separated by islets are shown in **Supplemental 5.** As expected, the
332 functional degree distributions for both $Cx36^{+/-}$ islets and $Cx36^{-/-}$ islets were increasingly right-skewed
333 (**Figure 6c, Supplemental 4a**), indicating a decrease in the average islet synchronization. Heterozygous
334 $Cx36^{+/-}$ islets demonstrated decreased average network degree (see **Table 1**) compared to wild-type
335 $Cx36^{+/+}$ islets (**Figure 6d**, **Figure 6a-c** middle vs. left), and homozygous $Cx36^{-/-}$ demonstrated further
336 decreased degree compared to both wild-type $Cx36^{+/+}$ islets (**Figure 6d**, **Figure 6a-c** right vs. left) and
337 $Cx36^{+/-}$ islets (**Figure 6d**, **Figure 6a-c** right vs. middle), further indicating that decreases in gap junction
338 conductance leads to decreases in [Ca^{2+}] oscillation synchronization (**Supplemental 4b**). Consistent
339 with this, substantially more cells in $Cx36^{+/-}$ islets (74% of cells) and $Cx36^{-/-}$ islets (93% of cells) were
340 not functionally connected to any other cell in the islet, compared to in $Cx36^{+/+}$ islets (40% of cells)
341 (**Figure 6e**). These data show that edges in the functional network become highly sparse as the structural
342 network decreases. It unlikely that these findings result from differences in network size across
343 genotypes as islets were of similar size ranges in each case (**Supplemental 3c**).
344 We next sought to quantify how the removal of edges in the structural network influences the
345 functional network topology (**Table 1**). Network topology statistics give us insight into how the network
346 functions. For example, c*lustering coefficient* (C_{avg}) is a local parameter that quantifies the percent of
347 nodes connected to a given node that are also connected to each other (**Table 1**). A local parameter is a
348 measure of the neighborhood of connections around an individual node. A high clustering coefficient in
349 the functional network would indicate that cells tend to synchronize with other cells that share some
350 property. The clustering coefficient of the functional networks decreased significantly as gap junction
351 coupling decreased, being significantly lower in $Cx36^{+/-}$ islets and $Cx36^{-/-}$ islets compared to $Cx36^{+/+}$

352 islets (**Figure 6f**). To statistically quantify whether the functional network topology is intentionally
353 organized or a result of random edge generation, we compared each metric with that determined from
354 one thousand random networks created with the same number of nodes, edges, and degree of
355 connectivity as the functional network of interest *(4, 7, 9)*. An example random graph is shown in **Table**
356 **1**. The relative overlap between the network characteristics from the islets of interest with those of a
357 random network describes the likelihood that the functional network of the islets could be created by
358 random chance, where random graphs have low clustering *(7)*. If the physical gap junctions are the
359 property that gives the functional network a high clustering coefficient, then reducing gap junction
360 coupling should result in a clustering coefficient closer to zero and be completely explained by the
361 random graph. For all islets, the clustering coefficient of the islet network was greater than that of a
362 random network $C_{avg} > C_{rand}$ (**Figure 6f,** box and whisker plot). Thus, in agreement with previous
363 results, this finding suggests that something other than the gap junction structural network contributes to
364 local properties of the functional network topology.

365 *Average shortest path length* (L_{avg}) is a global parameter defined as the average smallest number
366 of nodes required to traverse between any cell pair (**Table 1**). Global parameters define the connectivity
367 across the entire network. A random network or a regular network (see Table 1) with a few edges
368 randomly moved **(Table 1**) will have a small shortest path length. The normalized shortest path length
369 increased significantly as gap junction coupling decreased, and was significantly higher in $Cx36^{+/-}$ islets
370 and $Cx36^{-/-}$ islets compared to $Cx36^{+/+}$ islets **(Figure 6g**). For $Cx36^{+/+}$ islets, the measured shortest path
371 length was much greater than that of a random network ($L_{avg} > L_{rand}$). However, as gap junction
372 coupling decreased, the measured shortest path length showed a larger intersection with that of a random
373 network: for $Cx36^{-/-}$ islets all measured data points could be explained by random chance ($L_{avg} \approx$
374 L_{rand}). This finding suggests that the gap junction structural network contributes to global, long-range
375 properties of the functional network topology, similar to our findings in figure 4. *Global efficiency*, which
376 has previously been used to describe islet networks *(9)*, is related to the inverse of the shortest path length
377 (**Table 1**). Global efficiency significantly decreased with decreased gap junction coupling (**Figure 6h**).
378 Similar to path length, as gap junction coupling decreased, the measured global efficiency showed a
379 larger intersection with that of a random network.

380 The functional network in WT mice islets has been shown to contain *small-world qualities (9)*,
381 meaning that it exhibits the high clustering of a regular network and the high efficiency (short path
382 length) of a random network (**Table 1**). A small-word functional network is highly efficient to traverse
383 (along functional edges), but cells still tend to synchronize will other cells of similar attributes. From
384 such a network hubs arise. We sought to investigate whether these functional network small-world
385 qualities were diminished when structural edges were removed. Previously *(9)*, small-worldness was
386 quantified using random networks. However, as the functional network becomes more sparse, the
387 uncertainty in random network based approach increases (**Supplemental 4d,** seen more clearly in
388 **Supplemental 6d).** To remove this uncertainty, we used an alternative metric *(45)* which was formulated
389 specifically to analyze small world-ness in sparse networks. *Local efficiency* reveals how efficient the
390 communication is between neighbors of a node when that node is removed. Thus if both global efficiency
391 E_{global} and local efficiency E_{local} are large, the network has small world qualities *(45)*. There was a
392 significant decrease in local efficiency with reduced gap junction coupling, being significantly lower in
393 $Cx36^{+/-}$ islets and $Cx36^{-/-}$ islets compared to $Cx36^{+/+}$ islets (**Figure 6j).** These data show that as gap

junction coupling decreases, both global and local efficiency decrease and therefore small world-ness of the functional network decreases. Therefore reducing gap junction coupling decreases (but does not completely abolish) the communication efficiency of the islet. However, the fact that the random networks cannot explain the clustering of Cx36$^{-/-}$ indicates that other attributes are driving cellular synchronization, in agreement with our previous results.

Finally, to quantify the relationship between physical location and [Ca^{2+}] oscillation synchronization, we calculated the ratio between the average distance separating synchronized cells and the average distance separating all cells in the islet $\left(D = \frac{D_{sync}}{D_{all}}\right)$. If this ratio is less than one, it would indicate that cells tended to synchronize preferentially based on location. The average distance between synchronized cells compared to islet average was less than one for all but one Cx36$^{-/-}$ mouse **(Figure 6k)** and there was no significant difference between the three islet genotypes, suggesting that cells tend to synchronize to nearby cells but this is not fully dependent on gap junction coupling. These results together suggest that variations in physical gap junction coupling is not the only factor driving the synchronization of oscillatory [Ca^{2+}] dynamics. In all cases, these functional network characteristics did not show any significant mouse to mouse variability (**Supplemental 5**).

<u>Altering the gap junction structural network in the computational model agrees with experiments.</u>
Finally, we combined all three of our questions by investigating how changes in the structural network affect the functional network topology and relationships between function, structure, and metabolism. We simulated decreased structural edges by altering the average coupling conductance (g_{coup}) in our simulated islet. As expected, islets with reduced average g_{coup} showed reduced [Ca^{2+}] oscillation synchronization: simulated islets with average $g_{coup} = 0.12\ nS$ had higher synchronization than those with average $g_{coup} = 0.06\ nS$ or $0.03\ nS$ (**Figure 7a**). Similarly, following functional network analysis, the total number of functional network edges decreased as gap junction coupling was decreased (visualized in **Figure 7 a,b**), indicating that our simulated islet follows closely with experiments. The probability that two cells were connected in the functional network given that they were gap junction coupled (connected in the structural network, $\Pr(Sync|GJ)$) decreased significantly as gap junction coupling was decreased (**Figure 7c**). This indicates that as the gap junction conductance decreases and the network becomes sparser, the probability that two gap junction connected cells will be functionally connected decreases. Similarly, the probability that two cells were connected in the functional network given the cells had similar rates of glucose metabolism decreased as gap junction coupling decreased (**Figure 7d**). This indicates that gap junctions do play a role in synchronizing metabolically similar cells. Conversely, the probability of a gap junction connection given that two cells were synchronized in the functional network ($\Pr(GJ|Sync)$) increased as gap junction coupling decreased (**Figure 7e**). The probability of two cells showing similar rates of glucose metabolism given that two cells were connected in the functional network also increased as gap junction coupling decreased **(Figure 7f)** and showed higher probabilities ($0.2 - 0.3\ vs\ 0.1 - 0.2$) than that for $\Pr(Sync|GJ)$ in each case. These results indicates that as gap junction coupling decreases, a synchronized cell is more likely to be connected via a gap junction or metabolic similarity. However, this is not because the overlap between the two networks is larger but because the number of synchronized cells is smaller (**Figure 7b).** Together, these

results show that gap junctions are important for facilitating islet synchronization, but metabolism drives synchronization between individual cells given sufficient coupling.

We then quantified the three-dimensional stimulated functional network topology upon reduced gap junction conductance and compared these with network topology calculated from the two-dimensional calcium imaging data. The average degree significantly decreased as coupling decreased (**Figure 7g).** The clustering coefficient C_{avg} progressively decreased with decreasing gap junction conductance (**Figure 7e**). However, the clustering coefficient from the simulated islets was always substantially greater than that determined from a random network, with no overlap (**Figure 7e**). Global efficiency also progressively decreased with decreased gap junction conductance (**Figure 7i**). The global efficiency from the simulated islets was always less than that determined from a random network with no overlap (**Figure 7i**). These trends are similar to that of the experiments but the lack of overlap between random and measured global efficiency is more pronounced, likely due to having more cells from a three-dimensional view of the islet network. Also similar to our experimental observations the local efficiency decreased with gap junction conductance (**Figure 7j**). The decreases in both global efficiency and local efficiency with decreasing gap junction conductance indicate that the network strays away from small world properties as gap junction conductance decreases. This follows our experimental observations.

Discussion:

The old saying goes "cells that fire together, wire together." However, this has not been directly proven for every biological system. Further, it may be the case that cells that fire together have similar intrinsic excitatory characteristics that allows them to share dynamics. The primary aim of this study was to investigate the relationship between functional networks, structural networks, and underlying system dynamics of the β-cells in the pancreatic islet. We framed our study around three guiding questions. 1) Are subpopulations that emerge from the β-cells functional network differentiated by a unique location in the structural network or by intrinsic properties of the cells? 2) What does the islet functional network indicate about its underlying structure or intrinsic cell properties? 3) Can we fully explain the disruption in the functional network by the removal of nodes and edges in the structural network or are there other factors involved? **Figure 8** shows a graphical representation of the answers to these questions based on our data.

Calcium-based imaging is a common technique used to analyze cellular dynamics, identify cell subpopulations, and represent the system by functional networks. For this reason, most network-informed biological studies utilize synchronization-based functional networks to make conclusions about a system. This approach has yielded tremendous insight into how different subpopulations of cells can contribute to system dynamics *(9, 10, 27, 30, 32, 46)*. However, when discussing the loss of synchronization due to cell death or disruption in signaling, such as the case for many diseases, it is changes in the structural network (e.g., gap junctions, synapses, accumulation of plaque) that cause dysfunction. Therefore, it is important to understand the relationship between structural and functional networks. The islet of Langerhans is a relatively closed biological system with simple architecture that affords the opportunity for high fidelity experimental and computation analysis, making it an ideal system to answer biological network theory-based questions.

To make study more robust, we used both experimental and computational techniques. Computational modeling is beneficial as it allows us to carefully adjust and extract the exact system parameters, investigate the system explicitly, and quantify the entire three-dimensional network without noise. Experiments can then be used to verify model findings and trends on real-world data. This kind of joint analysis is important for robust, repeatable conclusions.

<u>1. Subpopulations of β-cells in the functional network are driven by metabolism more than gap junctions</u>

Our computational and experimental results show the existence of a subpopulation of highly synchronized cells within the islet, known as β-cell hubs *(10, 47)* **(Figure 1)**. β-cell hubs are identified as any cell whose degree from the functional network is >60% of the network maximum and they are characterized by a higher than average metabolic activity and the electrical signature of depolarizing before and repolarizing after the rest of the islet. The simulated β-cell hubs emerge from the network with the assumption that rate of glucose metabolism and gap junction coupling is independent of one another. Therefore, the dependency between rate of glucose metabolism and gap junction coupling seem to not be required for the existence of β-cell hubs. Interestingly, rate of glucose metabolism is associated with β-cell hubs more strongly than structural gap junction coupling. Computational studies showed a low correlation between gap junction coupling and synchronization, while experiments showed no trend. In contrast, experimental studies showed a clear correlation between cell degree in the functional

492 network and metabolic activity (reflected by NAD(P)H florescence) (**Figure 2)**. Semi-quantitative
493 immunofluorescence has indicated that β-cell hubs may show elevated metabolic activity due to elevated
494 glucokinase protein levels *(10)*. However, to our knowledge real-time quantification of metabolic
495 activity has not been correlated to cellular synchronization. Our results were validated experimentally.
496 Fluorescence recovery after photobleaching (FRAP) *(48)* provides a measurement for gap junction
497 permeability. By analyzing islets using both Ca^{2+}-based functional analysis and FRAP, our data showed
498 that highly synchronized cells do not have higher gap junction permeability (**Figure 2)**. *These*
499 *experimental findings support our computational findings that gap junctions are not the primary*
500 *distinguishing factor in determining variations in cellular synchronization.*

501 <u>2. Metabolic similarities drive the functional network</u>
502 Conditional probabilities quantify the relationship between the structural and functional networks at a
503 cell-to-cell basis. The probability of synchronization given gap junction connection (Pr(Sync|GJ))
504 addresses the question of whether cells connected an edge in the structural network are always connected
505 in the functional network. Unexpectedly, only ~40% of gap junction connected cells were considered
506 highly synchronized by functional network analysis (**Figure 3b)**. While it is a well-known fact that gap
507 junctions are required for islet-wide synchronization *(13)*, this finding suggests that other factors besides
508 just physical connections contribute to the high synchronization of individual cell pairs. The probability
509 of a gap junction given a synchronized cell pair (Pr(GJ|Sync)) addresses the assumption that
510 synchronization can be used to infer gap junctions. If this probability is high, then functional network
511 analysis can be used to directly infer the underlying gap junction structure. We found that Pr(Sync|GJ)
512 for five simulated islets was $< 5\%$, indicating that synchronization does not directly imply a gap junction
513 connection (**figure 3b)**. Interestingly, the probability that two synchronized cells had high average
514 metabolism or similar average metabolism was significantly larger than the probability of them sharing
515 a gap junction β-cell hubs(Figure 3e, f). This leads to the conclusion that elevated glucose metabolism,
516 rather than elevated gap junction coupling is driving high synchronization between individual cells. This
517 conclusion corresponds to our first finding that subpopulations of β-cells in the functional network are
518 driven by glucose metabolism to a greater degree than gap junction connections.
519 We also investigated whether a long-range connected cell pair in the functional network indicates
520 a chain of strongly coupled cells in the structural network (**Figure 4)**. While the electrical communication
521 between β-cells is not uni-directional, this analysis allows us to detect even the most minute influence
522 of gap junction paths on Ca^{2+} synchronization. Synchronized cells had a lower gap junction resistance
523 (or higher conductance) than non-synchronized cells however, the strong overlap in distributions
524 indicates that functionally connected long-range pair of cells do not always have a higher gap junction
525 conductance than a cell pair that does not share a functional connection. Interestingly, we also found that
526 longer-range cellular synchronization was more strongly correlated with the metabolic rate for up to 5
527 cells separation. These findings indicate that short to medium range synchronization is more reflective
528 of metabolic activity.
529 The surprising part of our findings is that gap junctions do not guarantee high synchronization
530 between a cell pair, as previously assumed *(28)*. We know that gap junctions facilitate ion passage
531 between cells to synchronize electrical oscillations. Therefore, it makes sense that long-range
532 synchronization requires a chain of highly conductive gap junctions, and that islet wide synchronization

533 is decreased when gap junctions are removed. However, we also know that in the case of electrically
534 active cells such as neurons or cells in the islet of Langerhans, gap junctions are not the primary factor
535 driving electrical activity. In β-cells, cell metabolism is responsible for driving electrical activity and
536 Ca^{2+} elevations, while gap junctions simply facilitate ion passage between cells to synchronize electrical
537 oscillations. Additionally, we know from electrophysiology that it is the individual cell's membrane
538 conductance, controlled in part by glucose metabolism, that determines the actual coupling current
539 strength *(30, 49)*. Prior experiments have also shown that cells that are preferentially activated by
540 optogenetic ChR2 stimulation were more metabolically active by NAD(P)H autofluorescence, but not
541 preferentially gap junction coupled *(38)*. Furthermore, gap junctions have a larger role in repolarizing
542 cells back to resting membrane potential compared to depolarizing cells to an elevated membrane
543 potential *(30)*; whereas metabolic activity is more influential in driving cellular depolarization.
544 Additionally, in a completely uncoupled network, cells with identical frequencies will still be
545 synchronized. Since the metabolic activity is highly influential in a cell's oscillatory frequency, it makes
546 sense that metabolic activity would be strongly influential in determining functional edges.

547 <u>3. Removal of edges in the structural network decreases functional efficiency and local connectivity</u>
548 While the functional network is not a direct replica of the structural network, previous studies show that
549 there is a relationship between the two *(13, 50)*. Genetically knocking out the Cx36 gap junction protein
550 in mice islets allows us to "remove" edges from the structural network. Previous studies have shown that
551 Cx36 deficiency in mice leads to slower calcium waves *(13)*, loss of calcium oscillations and
552 synchronization and loss of pulsatile insulin secretion *(15)*. In modeling studies, coupling strength was
553 shown to be anticorrelated with small worldness *(34)*.
554 In the computational model, neither clustering coefficient which reflects local properties of the
555 functional network, nor global efficiency which reflects global properties of the functional network could
556 be explained by randomness, even at the lowest g_{coup} β-cell hubs **(Figure 7)**. This result was similar to
557 experimental findings which *reflect* a single 2-dimensional plane whereas the computational model
558 reflects the entire 3-dimensional network. According to experiments by Watts and Strogatz *(4)*, only the
559 most ordered networks will show zero overlap with randomness between the clustering and efficiency
560 statistics. Our results are unexpected because if gap junctions were solely responsible for variations in
561 islet synchronization, a decrease in gap junction coupling would cause the functional network to appear
562 more random. Instead, this indicates that β-cells are preferentially, not randomly, synchronized even in
563 the presence of very low gap junction coupling. This synchronization is likely to be explained by other
564 intrinsic cellular properties of the β-cells, which supports our previous claim that gap junctions are not
565 the only factor important in determining variations in cellular synchronization. The high clustering
566 coefficient found experimentally in Cx36 knockout islets **(Figure 6)** and computationally with low g_{coup}
567 indicates that cells tend to be functionally connected (i.e., highly synchronized) independent of variations
568 in gap junctions. These results again contribute to the evidence that gap junction connections are not the
569 only driver of synchronization. Of note, the partial overlap between global efficiency between Cx36
570 knockout islets and a random network suggests that gap junctions play some role in maintaining long-
571 range functional connections. This is consistent with our computational measurements that show slightly
572 elevated gap junction conductance in long-range (>4 cells) connections between synchronized cells
573 compared to non-synchronized cells. Further, the significant decrease in both clustering coefficient and

global efficiency of the functional network with decreasing Cx36 expression and g_{coup} indicates that as structural gap junction connections are removed, the islet loses efficient signal propagation and high ability to synchronize, which likely has pathophysiological implications. For example, this decreased functional small worldness likely contributes to the lack of islet coordination and pulsatile insulin, in diseases such as diabetes, where gap junction coupling has been shown to decrease *(25, 26, 51)*. Islet coordination and pulsatile insulin release are essential for proper glucose homeostasis *(19–21)*.

Broader implications

We have shown evidence that the functional network of the islet of Langerhans is influenced by its underlying structure but is more reflective of intrinsic cellular metabolic activity than gap junction connections. Studies have shown that the hyper-polarization of highly synchronized β-cell hubs disproportionately disrupts islet calcium dynamics, but the actual removal of hubs does not *(30, 32)*. Our new perspective that β-cell hubs are uniquely defined by metabolic activity rather than gap junction coupling, helps explain these results. β-cell hubs drive synchronization across the islet because they are more metabolically active, not because they are more gap junction coupled. This perspective could also be utilized when studying calcium dynamics, with the new understanding that synchronization can give insight into cellular properties that drive excitability of the cell, such as the metabolic activity of β-cells. Further, perturbations in metabolism, such as metabolic stress that occurs in diabetes, may have a significant influence on the synchronization of the islet. While this study was conducted on experimental and computational representations of the islets of Langerhans, we suggest that these findings may be extrapolated to larger systems.

Potential Limitations

The most obvious limitation of this study, as for any computational study, is that computational models do not perfectly reflect reality. Our computational model is based on careful physiological recordings and has been previously validated *(38–40)*. We further address this limitation through experimental studies which agree well with results from these computational models. However, a strength in our use of the computational islet model is that all our results are internally derived. That is, even if the computational model is not fully reflective of the experimental islet, the functional and structural networks were obtained from the same model, so the relationship between them is not dependent on the models' ability to reflect islet dynamics (though we have shown that it does). This fact also allows our methods to translate to any oscillatory network with similar characteristics.

The choice of threshold when creating the functional network is influential in the results (**Supplemental 1**) and should be carefully considered in any use of synchronization to create the functional network. We picked our threshold to match that of the prior experimental results *(9, 10, 32)*. The computational threshold was very high ($R_{th} = 0.9995$) because, unlike experiments, the computational model had no noise, so the synchronization was more acute. However, the trends in our results were consistent across thresholds (**Supplemental 1)**.

Finally, in the islet computational model we analyze only fast electrical oscillations, whose frequency are less than 1 minute *(52)*. A similar analysis should eventually be done considering slower metabolic oscillations and factoring in the (currently unknown) mechanism by which these metabolic oscillations may be synchronized across the islet. We also assume that gap junction connections between cells are constant throughout the time of analysis. Finally, the islet also contains α, δ, γ, and other cell

types which have been shown to influence β-cell dynamics through a number of mechanisms *(53–55)*. This study only analyzes β-cells which is the common practice among other network studies which we compare to *(9, 10, 31)*. However, we cannot exclude long-range structural projections from δ cells *(56, 57)* and that δ cells may be gap junction coupled *(59)*. In the future, network analysis should be applied to include other cell types as it could give valuable insight how their interactions can shape the overall islet response to nutrient changes.

Conclusions:

In this study, we investigate the relationship between the synchronization-based functional network and the structural network formed by gap junctions, within the β-cells in the islets of Langerhans. We conclude with three major points. *First*, highly connected subpopulations of β-cells, including β-cell hubs are driven by metabolism more than gap junctions. *Second*, metabolic similarities rather than gap junctions drive edges in the functional network of the islet. *Third,* removal of edges in the structural network decreases global communication efficiency and local connectivity. Specifically, we show that decreasing gap junction conductance causes the functional network to become more sparse and less small world-like, which can have pathophysiologic implications. These results provide insight into understanding the relationship between function and structure in islet networks and biological networks as a whole.

633 **Methods:**

634 Calcium imaging, FRAP, and NAD(P)H

635 Animal care: Male and female mice were used under protocols approved by the University of Colorado
636 Institutional Animal Care and Use Committee. β-cell-specific GCaMP6s expression (β-GCaMP6s) was
637 achieved through crossing a MIP-CreER (The Jackson Laboratory) and a GCaMP6s line (The Jackson
638 Laboratory)*(26)*. Genotype was verified through qPCR (Transetyx, Memphis, TN). Mice were held in a
639 temperature-controlled environment with a 12 h light/dark cycle and given continuous access to food
640 and water. CreER-mediated recombination was induced by 5 daily doses of tamoxifen (50mg/kg bw in
641 corn oil) delivered IP.

642 Islet isolation and culture: Islets were isolated from mice under ketamine/xylazine anesthesia (80 and 16
643 mg/kg) by collagenase delivery into the pancreas via injection into the bile duct. The collagenase-
644 inflated pancreas was surgically removed and digested. Islets were handpicked and planted into the glass-
645 bottom dishes (MatTek) using CellTak cell tissue adhesive (Sigma-Aldrich). Islets were cultured in
646 RPMI medium (Corning, Tewksbury, MA) containing 10% fetal bovine serum, 100 U/mL penicillin,
647 and 100 mg/mL streptomycin. Islets were incubated at 37C, 5% CO2 for 24-72 h before imaging.

648 Imaging: An hour prior to imaging nutrition media from the isolated islets was replaced by an imaging
649 solution (125 mM NaCl, 5.7 mM KCl, 2.5 mM CaCl2, 1.2 mM MgCl2, 10 mM HEPES, and 0.1% BSA,
650 pH 7.4) containing 2 mM glucose. During imaging the glucose level was raised to 11mM. Islets were
651 imaged using either a LSM780 system (Carl Zeiss, Oberkochen, Germany) with a 40x 1.2 NA objective
652 or with an LSM800 system (Carl Zeiss) with 20x 0.8 NA PlanApochromat objective, or a 40x 1.2 NA
653 objective, with samples held at 37C.

654 For [Ca^{2+}] measurements GCaMP6s fluorescence was excited using a 488-nm laser. Images were
655 acquired at 1 frame/s at 10-20 m depth from the bottom of the islet. Glucose was elevated 3 minutes
656 after the start of recording, unless stated otherwise.

657 NAD(P)H autofluorescence and [Ca^{2+}] dynamics were performed in the same z-position within
658 the islet. NADH(P)H autofluorescence was imaged under two-photon excitation using a tunable mode-
659 locked Ti:sapphire laser (Chameleon; Coherent, Santa Clara, CA) set to 710 nm. Fluorescence emission
660 was detected at 400–450 nm using the internal detector. Z-stacks of 6–7 images were acquired spanning
661 a depth of 5 μm. First the NAD(P)H was recorded at 2 mM glucose, then the [Ca^{2+}] dynamics was
662 recorder at 2 mM and during transition to 11 mM glucose. After the [Ca^{2+}] wave was established, the
663 NAD(P)H was recorded at 11 mM glucose.

664 Cx36 gap junction permeability and [Ca^{2+}] dynamics were performed in the same z-position
665 within the islet, with gap junction permeability measured using fluorescence recovery after
666 photobleaching (FRAP), as previously described *(43)*. After [Ca^{2+}] imaging, islets were loaded with 12
667 mM Rhodamine-123 for 30 min at 37C in imaging solution. Islets were then washed and FRAP
668 performed at 11mM glucose at room temperature. Room temperature was used because at this
669 temperature the Rhodamine-123 travels between the cells only through the Cx36 gap junctions, versus
670 at 37 C it can permeate a cell membrane. Rhodamine-123 was excited using a 488-nm laser line, and
671 fluorescence emission was detected at 500–580 nm. Three baseline intensity images were initially
672 recorded. A region of interest was then photobleached achieving, on average, a 50% decrease in
673 fluorescence, and images were then acquired every 5-15 s for 15-30 min.

674 Analysis of [Ca2+] dynamics: Pearson-product-based network analysis presented in Figure 2 was
675 performed as previously reported *(9)*. [Ca^{2+}] time courses were analyzed during the second-phase [Ca^{2+}]
676 response, when the slow calcium wave was established. The Pearson product for each cell pair in the
677 islet was calculated over each time point, and the time-average values were computed to construct a
678 correlation matrix. An adjacency matrix was calculated by applying a threshold to the correlation matrix.
679 The same threshold of 0.9 was applied to all islets. All cell pairs with a non-zero values in the adjacency
680 matrix were considered to have a functional edge. The percent of edges was calculated with respect to
681 the maximum number of edges per cell in each individual islet. For example, if a most connected cell
682 possessed max=10 edges, and other cells had 1, 3, …7 edges – then the % were: 10%, 30%, …70%.
683
684 <u>Prior calcium imaging first presented in (13)</u>

685 Islet isolation: Islets were isolated as described in Scharp et al. (60) and Stefan et al. (61) and maintained
686 in Roswell Park Memorial. Institute medium containing 10% fetal bovine serum, 11 mM glucose at 37C
687 under humidified 5% CO2 for 24–48 h before imaging.

688 Imaging islets: Isolated islets were stained with 4 mM Fluo-4 AM (Invitrogen, Carlsbad, CA) in imaging
689 medium (125 mM NaCl, 5.7 mM KCl, 2.5 CaCl2, 1.2 mM MgCl2, 10 mM HEPES, 2mM glucose, 0.1%
690 bovine serum albumin, pH 7.4) at room temperature for 1–3 h before imaging. Islets were imaged in a
691 polydimethylsiloxane (PDMS) microfluidic device, the fabrication of which has been previously
692 described in Rocheleau et al. , which holds the islet stable for imaging and allows rapid reagent change,
693 such as varying glucose stimulation or adding gap junction inhibitors. Fluo-4 fluorescence is imaged 15
694 min after a step increase in glucose from low (2 mM) to high (11 mM). High speed imaging is performed
695 on an LSM5Live with a 203 0.8 NA Fluar Objective (Zeiss, Jena, Germany) using a 488 nm diode laser
696 for excitation and a 495 nm long-pass filter to detect fluorescence emission. The microfluidic device is
697 held on the microscope stage in a humidified temperature-controlled chamber, maintained at 37 C.
698 Images were acquired at a rate of 4–6 frames per second, with average powers at the sample being
699 minimized to, 200 mW/cm2.

700 Analysis of Ca2+ Imaging data: We present data from 11 Islets from 6 WT mice, 11 Islets from 11
701 heterozygous Cx36 +/− knockout mice, and 14 Islets from 3 homozygous Cx36 -/- knockout mice. We
702 extracted cell calcium dynamics by visually identifying and circling all cells in the islet. We assumed
703 that the pixels within a cell should be well coordinated, so we removed any pixels whose dynamics were
704 not within 5-10 STD of the average. This usually resulted in the removal of 1-5 pixels on the edge of the
705 cell boundary.

706 Threshold: Previous studies have shown that wild type Islets should have a degree distribution that is
707 roughly linear when plotted on a log-log plot and average degree of either 8 or between 5-15 *(9, 10, 32,*
708 *63)* . To determine R_{th} that best satisfied both of these findings, we utilized constrained optimization
709 matlab algorithm fminsearchbnd*(64)* to find the $R_{th_{opt}}$ which maximized the goodness of fit to a power
710 law distribution, while forcing $5 \leq k_{avg} \leq 15$ for each WT Islet constrained optimization. The average
711 optimal threshold ($R_{th} = 0.90$).

712 Average distance between connected cells: The average distance between connected cells calculated the
713 total number of pixels between the center of two connected cells. The average distance was expressed
714 as the normalized distance between connected cells and the average distance between all cells in the Islet
715 to control for image and Islet size.

716 Computational Model:

717 This ordinary differential equation model has been described previously (30) and validated on
718 experimental studies (38–41). It is based on a single β-cell electrophysiologic model (65), in which the
719 membrane potential (V_i) for β-cell$_i$ is solved for each time step using eq 1a. We created a 1000 β-cell
720 network and electrically coupled any cell pairs within a small distance from each other. We chose 1000
721 β-cell because most species (including human and mouse) contain on average 1000 β-cells in an islet
722 (66) and it is the number which has been validated experimentally. The coupling current, I_{coup} is
723 determined by the difference in voltage between the cell pair and the average coupling conductance
724 (g_{coup}) between them (1b). All code was written in C++ and run on the SUMMIT supercomputer
725 (University of Colorado Boulder). All simulations are run at 11mMol glucose. The membrane potential
726 (V_i) for β-cell$_i$ is solved for using the ODE:

$$C_m \frac{dV_i}{dt} = I_{Cav} + I_{TRPM} + I_{SOC} + I_{bNSC} + I_{KDr} + I_{KCa(SK)} + I_{K_{ATP}} + I_{NaCa} + I_{PMCA} + I_{NaCa} + I_{Coup} \quad (1a)$$

$$I_{Coup} = \sum_i g_{coup}^{ij}(V_i - V_j) \quad (1b)$$

727 The average number of gap junction connections per cell was 5.24. Cellular heterogeneity was
728 introduced by assigning randomized metabolic and electrical parameter values to each cell based on their
729 distributions previously determined by experimental studies. For example, coupling conductance (g_{coup})
730 was assigned so that the Islet average is $g_{coup} = 0.12nS$ and glucokinase (k_{glyc}), the rate-limiting step
731 in glycolysis, was assigned so that the average $k_{glyc} = 1.26 * 10^{-04}\ sec^{-1}$. We ran the simulation for
732 500 seconds and only the 2nd phase was analyzed, in concordance with *(10)*. All the results presented are
733 based on five different Islets with randomized parameter values. β-cell heterogeneity was simulated by
734 randomizing parameters including coupling conductance (g_{coup}) and metabolic rate (k_{glyc}) according
735 to experimental results. To explore the effects of coupling conductance on the functional network, we
736 altered Islet average coupling conductivity to $g_{coup} = 0.06\ nS$ and $g_{coup} = 0.03\ nS$, and then assigning
737 each cell a randomized g_{coup} based on the new target average. The gap junction conductance (g_{coup}) for
738 any cell was calculated as the sum of the average conductivity (g_{coup}) between the cell of interest and
739 any cells it shares a gap junction connection with:

740 $$g_{coup_j} = \sum_{i=1}^{m} \frac{1}{2} (g_{coup}^{i} + g_{coup}^{j})$$

741

742 Network Analysis:

743 *Creating Functional Network from simulated Islet:* The methodology was based on that previously
744 defined in *(9)*. First, the correlation coefficient between each cell was calculated using corr() function in
745 matlab, which follows equation: $R_{ij} = \frac{\sum[\bar{x}_i - x_i(t)][\bar{x}_j - x_j(t)]}{s_{x_i} s_{x_j}}$. Next, a threshold ($R_{th}$) was defined to
746 determine whether each cell pair is 'synchronized' or 'not synchronized'. For computational
747 experiments, the threshold was chosen such that the network roughly followed a power law distribution,
748 as predicted in *(9, 10)*. Unless otherwise noted, $R_{th} = 0.9995$ for computational analysis.

749 *Creating the Metabolic network:* Because gap junctions enforce localization onto the analysis, we looked
750 at cell pairs whose Pythagorean distance was $\leq 15\%$ of the Islet. Within this sample space, we looked
751 at cell pairs whose average k_{glyc} was higher than the Islet average (**Figure 4b**, green) ($0.5 *$
752 $\left|k_{glyc_i} + k_{glyc_j}\right| > average(0.5 * \left|k_{glyc_i} + k_{glyc_j}\right| \forall_{i_j})$), and cell pairs whose K_{glyc} was more similar
753 than the islet average ($\left|k_{glyc_i} - k_{glyc_j}\right| < average(\left|k_{glyc_i} - k_{glyc_j}\right| \forall_{i_j})$). We chose these parameters
754 such that the $Pr(Sync|GJ) = Pr\ (Sync|Met)$, which acts as a control allowing us to directly compare
755 $Pr(GJ|Sync)$ to $\Pr(Met|Sync)$.

756 *Average degree:* The degree k_i was calculated by counting the number of connections for $cell_i$ and
757 averaging k over all cells in the Islet, then normalized to the Islet size to remove any size dependence
758 ($\frac{k_{avg}}{n}, where\ n\ \equiv islet\ size$).

759 *Degree Distribution:* The degree distribution was calculated by first calculating the degree of each cell
760 by taking the column sum of the adjacency matrix. Then each cell degree was normalized by dividing
761 by the maximum degree in the Islet. The histogram was then calculated using GraphPad Prism.

762 *Hub identification:* In accordance with , any cell with more than 60% of the Islet's connections,
763 calculated by the degree distribution, was considered a hub cell.

764

765 Probabilities:

766 We first created the functional network and structural (GJ related probabilities) or metabolic network
767 (metabolism). We then calculated the probability that two cells were synchronized by:

768 $$\Pr(sync) = \frac{\frac{m_{sync}}{(n-1) * n}}{2}$$

769 Where m_{sync} = number of edges in the synchronized network, and n = number of nodes. Similarly, we
770 calculated the probability that two cells were either gap junction coupled or metabolically related using

771 $$\Pr(GJ\ or\ k_{glyc}) = \frac{\frac{m_{GJ\ or\ k_{glyc}}}{(n-1) * n}}{2}$$

772 Where $m_{GJ\ or\ k_{glyc}}$ is the number of edges in the gap junction or metabolic network.

To find the probability that a cell pair was both synchronized and GJ or metabolically connected, we calculated

$$\Pr(both) = \frac{\frac{m_{both}}{(n-1)*n}}{2}$$

Where m_{both} is any edge that exists in both matrices.

Finally, we calculated conditional probabilities by:

$$\Pr(sync|GJ) = \frac{\Pr(both)}{\Pr(GJ)}$$

$$\Pr(GJ|sync) = \frac{\Pr(both)}{\Pr(sync)}$$

These quantities were calculated separately for each Islet seed and then averaged.

Network topology analysis:

Shortest weighted path length: The gap junction network was weighted using the inverse of g_{coup} or k_{glyc} between $Cell_i$ and $Cell_i$: $W_{ij} = \frac{1}{\frac{1}{2}(g_{coup_i}+g_{coup_j})}$ or $W_{ij} = \frac{1}{\frac{1}{2}(k_{glyc_i}+k_{glyc_j})}$. This is done because the shortest path length algorithm views weights as "resistance" and finds the path of least resistance. The shortest weighted path between every cell was calculated using Johnson's algorithm (67). Cell pairs were then categorized as synchronized or not synchronized if their correlation coefficient was $< R_{th}$. The average for synchronized and non-synchronized cells was calculated over each Islet for each distance. To normalize over distance, each data point was divided by the average of the non-synchronized and synchronized islets for the given distance.

Clustering Coefficient: The clustering coefficient represents the 'cliquishness' of the network . This is defined by *(9)* as the "number of existing connections between all neighbors of a node, divided by the number of all possible connections between them." This was calculated by making a subgraph of each cell's connections and counting the number of connections between those cells. For example, if A is connected to B, C, and D, and B and C are connected but D is not connected to any other cell (see matrix). Then the clustering for cell A is $\frac{2}{3*2} = \frac{1}{3}$. Each node is a assigned a clustering coefficient C such that:

Subgraph - A	**B**	**C**	**D**
B		1	0
C	1		0
D	0	0	

The average clustering coefficient is $C_{avg} = \frac{1}{n}\sum_i^n C_i$.

Average Shortest Path Length: Shortest path length was calculated with matlab function graphallshortestpaths(). This function uses the Johnson's algorithm *(67)* to find the shortest path between every pair of cell in the Islet. For example, the path length between $cell_i$ and $cell_j$ is 1 if they are directly synchronized, or 2 if $cell_i$ is not synchronized with $cell_j$ but each is synchronized with $cell_k$. To compensate for highly sparse network, any non-connected node was given a characteristic path length

of $n+1$. Finally, the characteristic path length (L), or average path length, was expressed as the sum of all path lengths normalized to total possible connections (size*(size-1)).

The normalized average shortest path length (Supplemental 2d) is therefore calculated as $L_{avg} = \frac{1}{n}\frac{1}{n}\sum_{i=1}^{n}\sum_{j=1}^{n} L_{ij}$. To compensate for any non-connected cell, whose path length $L_{ix} = \infty$, where x is any cell in the Islet, we set the path length for non-connected cells to $L_{ix} \rightarrow n+1$ where n is the number of cells in the Islet.

Global Efficiency: The global efficiency is related to the inverse of global path length *(45)*.

$$\boldsymbol{E}_{\{\boldsymbol{global}\}} = \frac{1}{Islet_{size} * (Islet_{size} - 1)} \sum_{jk} \frac{1}{L_{jk}}$$

length using $E_{global} = \frac{1}{n(n-1)}\sum_{i=1}^{n}\sum_{j=1}^{n}\frac{1}{L_{ij}}$. Because $E_{global} = 0$ for a non-connected cell, the disconnected network is naturally compensated for.

Random Networks: Random networks were created using an Erodos Renyi approach (68). For each Islet, we created 1000 random networks with equal number of nodes, edges, and average degree as the Islet of interest. The probability that two cells were connected was given by $P = \frac{k_{avg}}{n}$. For each cell pair within the Islet, a random number generator created a number from 0-1. If that number was below P, those cells were connected by an edge.

Small World properties: For each Islet, small world parameters S_E and S_L were calculated 1000 times based on the 1000 random networks.

$$S_L = \frac{\frac{C_{avg}}{C_{rand}}}{\frac{L_{avg}}{L_{rand}}}$$

$$S_E = \frac{\frac{C_{avg}}{C_{rand}}}{\frac{E_{rand}}{E_{avg}}}.$$

Local Efficiency: Local efficiency is calculated by first extracting a subgraph based on the connections for an individual cell. Within that cell, the efficiency is calculated by:

$$E = \frac{1}{n_i * (n_i - 1)} \sum \frac{1}{L_{j,k}}$$

Where n_i is the number of nodes that an individual node is connected to. This is done for every node in the network and all efficiencies are averaged to present the local efficiency of the network.

<u>Significance Testing:</u>

Significance tests are done in Prism (GraphPad).

The computational model is run on 5 seeds, therefore all significance tests are paired.

Figure 1e-g, Figure 4e&h, and Figure 5c-f are paired, two tailed t-tests.

Figure 3e,f are repeated measures paired one-way ANOVA with multiple comparison using Tukey's multiple comparison.

Figure 4i,j are multiple paired t-tests with Bonferroni-Dunn adjustment.

All significance tests in figure 6 are unpaired ordinary one-way ANOVA tests.

Figure 7 c-j are ordinary paired one-way ANOVA with Tukey multiple comparison test.

Supplemental 1b and 2b, Figure 4 i and j and Figure 5i: To compare, we used a paired T-test with Bonferroni multiple comparisons corrections. Since we there were 15 cell distances, we set the significance threshold $\alpha = 0.003$. For convenience, we present asterisks next to significant P-values.

Supplemental 4b and c are two way ANOVA with Sidak's multiple comparisons

References

1. M. Koutrouli, E. Karatzas, D. Paez-Espino, G. A. Pavlopoulos, A guide to conquer the biological network era using graph theory. *Frontiers in bioengineering and biotechnology* **8**, 34 (2020).

2. S. H. Strogatz, Exploring complex networks. *Nature* **410**, 268–276 (2001).

3. M. E. Newman, The structure and function of complex networks. *SIAM review* **45**, 167–256 (2003).

4. D. J. Watts, S. H. Strogatz, Collective dynamics of 'small-world'networks. *nature* **393**, 440–442 (1998).

5. C. W. Lynn, D. S. Bassett, The physics of brain network structure, function and control. *Nature Reviews Physics* **1**, 318–332 (2019).

6. E. Bullmore, O. Sporns, Complex brain networks: graph theoretical analysis of structural and functional systems. *Nature reviews neuroscience* **10**, 186–198 (2009).

7. M. Newman, *Networks* (Oxford university press, 2018).

8. D. R. Chialvo, Emergent complex neural dynamics. *Nature physics* **6**, 744–750 (2010).

9. A. Stožer, M. Gosak, J. Dolenšek, M. Perc, M. Marhl, M. S. Rupnik, D. Korošak, Functional connectivity in islets of Langerhans from mouse pancreas tissue slices. *PLoS Comput Biol* **9**, e1002923 (2013).

10. N. R. Johnston, R. K. Mitchell, E. Haythorne, M. P. Pessoa, F. Semplici, J. Ferrer, L. Piemonti, P. Marchetti, M. Bugliani, D. Bosco, others, Beta cell hubs dictate pancreatic islet responses to glucose. *Cell metabolism* **24**, 389–401 (2016).

11. D. J. Hodson, M. Schaeffer, N. Romanò, P. Fontanaud, C. Lafont, J. Birkenstock, F. Molino, H. Christian, J. Lockey, D. Carmignac, others, Existence of long-lasting experience-dependent plasticity in endocrine cell networks. *Nature communications* **3**, 1–10 (2012).

12. C. Grienberger, A. Konnerth, Imaging calcium in neurons. *Neuron* **73**, 862–885 (2012).

13. R. K. Benninger, M. Zhang, W. S. Head, L. S. Satin, D. W. Piston, Gap junction coupling and calcium waves in the pancreatic islet. *Biophysical journal* **95**, 5048–5061 (2008).

14. V. Serre-Beinier, S. Le Gurun, N. Belluardo, A. Trovato-Salinaro, A. Charollais, J.-A. Haefliger, D. F. Condorelli, P. Meda, Cx36 preferentially connects beta-cells within pancreatic islets. *Diabetes* **49**, 727–734 (2000).

15. M. A. Ravier, M. Güldenagel, A. Charollais, A. Gjinovci, D. Caille, G. Söhl, C. B. Wollheim, K. Willecke, J.-C. Henquin, P. Meda, Loss of connexin36 channels alters β-cell coupling, islet synchronization of glucose-induced Ca2+ and insulin oscillations, and basal insulin release. *Diabetes* **54**, 1798–1807 (2005).

875 16. R. K. Benninger, V. Kravets, The physiological role of β-cell heterogeneity in pancreatic islet
876 function. *Nature Reviews Endocrinology* **18**, 9–22 (2022).

877 17. J. Weitz, D. Menegaz, A. Caicedo, Deciphering the Complex Communication Networks That
878 Orchestrate Pancreatic Islet Function. *Diabetes* **70**, 17–26 (2021).

879 18. W. S. Head, M. L. Orseth, C. S. Nunemaker, L. S. Satin, D. W. Piston, R. K. Benninger, Connexin-
880 36 gap junctions regulate in vivo first-and second-phase insulin secretion dynamics and glucose
881 tolerance in the conscious mouse. *Diabetes* **61**, 1700–1707 (2012).

882 19. N. Pørksen, M. Hollingdal, C. Juhl, P. Butler, J. D. Veldhuis, O. Schmitz, Pulsatile insulin
883 secretion: detection, regulation, and role in diabetes. *Diabetes* **51**, S245–S254 (2002).

884 20. A. V. Matveyenko, D. Liuwantara, T. Gurlo, D. Kirakossian, C. Dalla Man, C. Cobelli, M. F.
885 White, K. D. Copps, E. Volpi, S. Fujita, others, Pulsatile portal vein insulin delivery enhances hepatic
886 insulin action and signaling. *Diabetes* **61**, 2269–2279 (2012).

887 21. P. Bratusch-Marrain, M. Komjati, W. Waldhäusl, Efficacy of pulsatile versus continuous insulin
888 administration on hepatic glucose production and glucose utilization in type I diabetic humans.
889 *Diabetes* **35**, 922–926 (1986).

890 22. L. S. Satin, P. C. Butler, J. Ha, A. S. Sherman, Pulsatile insulin secretion, impaired glucose
891 tolerance and type 2 diabetes. *Mol Aspects Med* **42**, 61–77 (2015).

892 23. D. J. Hodson, R. K. Mitchell, E. A. Bellomo, G. Sun, L. Vinet, P. Meda, D. Li, W.-H. Li, M.
893 Bugliani, P. Marchetti, others, Lipotoxicity disrupts incretin-regulated human β cell connectivity. *The*
894 *Journal of clinical investigation* **123**, 4182–4194 (2013).

895 24. D. A. Lang, D. Matthews, M. Burnett, R. Turner, Brief, irregular oscillations of basal plasma
896 insulin and glucose concentrations in diabetic man. *Diabetes* **30**, 435–439 (1981).

897 25. J. R. St Clair, M. J. Westacott, N. L. Farnsworth, V. Kravets, W. E. Schleicher, J. G. Miranda, A.
898 Heintz, N. W. Ludin, R. K. Benninger, Restoring connexin-36 function in diabetogenic environments
899 precludes mouse and human islet dysfunction. *bioRxiv* (2020).

900 26. M. E. C. do Amaral, V. Kravets, J. M. Dwulet, N. L. Farnsworth, R. Piscopio, W. E. Schleicher, J.
901 G. Miranda, R. K. Benninger, Caloric Restriction recovers impaired β-cell-β-cell coupling, calcium
902 oscillation coordination and insulin secretion in prediabetic mice. *bioRxiv* (2020).

903 27. M. Gosak, R. Markovič, J. Dolenšek, M. S. Rupnik, M. Marhl, A. Stožer, M. Perc, Network
904 science of biological systems at different scales: A review. *Physics of life reviews* **24**, 118–135 (2018).

905 28. R. Markovič, A. Stožer, M. Gosak, J. Dolenšek, M. Marhl, M. S. Rupnik, Progressive glucose
906 stimulation of islet beta cells reveals a transition from segregated to integrated modular functional
907 connectivity patterns. *Sci Rep* **5**, 7845 (2015).

29. A. D. Broido, A. Clauset, Scale-free networks are rare. *Nature communications* **10**, 1–10 (2019).

30. J. M. Dwulet, J. K. Briggs, R. K. P. Benninger, Small subpopulations of beta-cells do not drive islet oscillatory [Ca2+] dynamics via gap junction communication. *PLOS Computational Biology* **17**, e1008948 (2021).

31. C.-L. Lei, J. A. Kellard, M. Hara, J. D. Johnson, B. Rodriguez, L. J. Briant, Beta-cell hubs maintain Ca2+ oscillations in human and mouse islet simulations. *Islets* **10**, 151–167 (2018).

32. D. Korošak, M. Jusup, B. Podobnik, A. Stožer, J. Dolenšek, P. Holme, M. S. Rupnik, Autopoietic influence hierarchies in pancreatic β-cells. *arXiv:2101.02255 [cond-mat, physics:physics]* (2021) (available at http://arxiv.org/abs/2101.02255).

33. L. S. Satin, Q. Zhang, P. Rorsman, "Take Me To Your Leader": An Electrophysiological Appraisal of the Role of Hub Cells in Pancreatic Islets. *Diabetes* **69**, 830–836 (2020).

34. J. P. Hogan, B. E. Peercy, Flipping the switch on the hub cell: Islet desynchronization through cell silencing. *PloS one* **16**, e0248974 (2021).

35. G. A. Rutter, N. Ninov, V. Salem, D. J. Hodson, Comment on Satin et al."Take me to your leader": an electrophysiological appraisal of the role of hub cells in pancreatic islets. Diabetes 2020; 69: 830–836. *Diabetes* **69**, e10–e11 (2020).

36. L. S. Satin, P. Rorsman, Response to comment on satin et al."Take me to your leader": An electrophysiological appraisal of the role of hub cells in pancreatic islets. Diabetes 2020; 69: 830–836. *Diabetes* **69**, e12–e13 (2020).

37. B. E. Peercy, A. S. Sherman, Do oscillations in pancreatic islets require pacemaker cells? *Journal of Biosciences* **47**, 1–11 (2022).

38. M. J. Westacott, N. W. Ludin, R. K. Benninger, Spatially organized β-cell subpopulations control electrical dynamics across islets of Langerhans. *Biophysical journal* **113**, 1093–1108 (2017).

39. J. M. Dwulet, N. W. Ludin, R. A. Piscopio, W. E. Schleicher, O. Moua, M. J. Westacott, R. K. Benninger, How heterogeneity in glucokinase and gap-junction coupling determines the islet [Ca2+] response. *Biophysical journal* **117**, 2188–2203 (2019).

40. T. H. Hraha, M. J. Westacott, M. Pozzoli, A. M. Notary, P. M. McClatchey, R. K. Benninger, Phase transitions in the multi-cellular regulatory behavior of pancreatic islet excitability. *PLoS computational biology* **10**, e1003819 (2014).

41. A. M. Notary, M. J. Westacott, T. H. Hraha, M. Pozzoli, R. K. P. Benninger, Decreases in Gap Junction Coupling Recovers Ca2+ and Insulin Secretion in Neonatal Diabetes Mellitus, Dependent on Beta Cell Heterogeneity and Noise. *PLOS Computational Biology* **12**, e1005116 (2016).

42. V. Salem, L. D. Silva, K. Suba, E. Georgiadou, S. N. M. Gharavy, N. Akhtar, A. Martin-Alonso, D. C. Gaboriau, S. M. Rothery, T. Stylianides, others, Leader beta-cells coordinate Ca 2+ dynamics across pancreatic islets in vivo. *Nature Metabolism* **1**, 615–629 (2019).

43. N. L. Farnsworth, A. Hemmati, M. Pozzoli, R. K. Benninger, Fluorescence recovery after photobleaching reveals regulation and distribution of connexin36 gap junction coupling within mouse islets of Langerhans. *The Journal of physiology* **592**, 4431–4446 (2014).

44. G. Cappon, M. G. Pedersen, Heterogeneity and nearest-neighbor coupling can explain small-worldness and wave properties in pancreatic islets. *Chaos: An Interdisciplinary Journal of Nonlinear Science* **26**, 053103 (2016).

45. V. Latora, M. Marchiori, Efficient behavior of small-world networks. *Physical review letters* **87**, 198701 (2001).

46. M. T. Adams, J. M. Dwulet, J. K. Briggs, C. A. Reissaus, E. Jin, J. M. Szulczewski, M. R. Lyman, S. M. Sdao, V. Kravets, S. D. Nimkulrat, others, Reduced synchroneity of intra-islet Ca2+ oscillations in vivo in Robo-deficient β cells. *Elife* **10** (2021).

47. R. K. Benninger, D. J. Hodson, New understanding of β-cell heterogeneity and in situ islet function. *Diabetes* **67**, 537–547 (2018).

48. N. L. Farnsworth, R. K. Benninger, New insights into the role of connexins in pancreatic islet function and diabetes. *FEBS letters* **588**, 1278–1287 (2014).

49. R. Plonsey, R. C. Barr, A. Bioelectricity, *Quantitative Approach* (Springer, 2007).

50. A. Sherman, J. Rinzel, Model for synchronization of pancreatic beta-cells by gap junction coupling. *Biophysical journal* **59**, 547–559 (1991).

51. N. L. Farnsworth, R. L. Walter, A. Hemmati, M. J. Westacott, R. K. Benninger, Low level pro-inflammatory cytokines decrease connexin36 gap junction coupling in mouse and human islets through nitric oxide-mediated protein kinase Cδ. *Journal of Biological Chemistry* **291**, 3184–3196 (2016).

52. R. Bertram, A. Sherman, L. S. Satin, Electrical bursting, calcium oscillations, and synchronization of pancreatic islets. *The Islets of Langerhans* , 261–279 (2010).

53. J.-C. Henquin, Paracrine and autocrine control of insulin secretion in human islets: evidence and pending questions. *American Journal of Physiology-Endocrinology and Metabolism* **320**, E78–E86 (2021).

54. T. Moede, I. B. Leibiger, P.-O. Berggren, Alpha cell regulation of beta cell function. *Diabetologia* **63**, 2064–2075 (2020).

971 55. T. Van Der Meulen, C. J. Donaldson, E. Cáceres, A. E. Hunter, C. Cowing-Zitron, L. D. Pound, M.
972 W. Adams, A. Zembrzycki, K. L. Grove, M. O. Huising, Urocortin3 mediates somatostatin-dependent
973 negative feedback control of insulin secretion. *Nature medicine* **21**, 769–776 (2015).

974 56. R. Arrojo e Drigo, S. Jacob, C. F. García-Prieto, X. Zheng, M. Fukuda, H. T. T. Nhu, O.
975 Stelmashenko, F. L. M. Peçanha, R. Rodriguez-Diaz, E. Bushong, others, Structural basis for delta cell
976 paracrine regulation in pancreatic islets. *Nature communications* **10**, 1–12 (2019).

977 57. L. Briant, T. Reinbothe, I. Spiliotis, C. Miranda, B. Rodriguez, P. Rorsman, δ-cells and β-cells are
978 electrically coupled and regulate α-cell activity via somatostatin. *The Journal of physiology* **596**, 197–
979 215 (2018).

980 58. R. A. e Drigo, S. Jacob, C. F. García-Prieto, X. Zheng, M. Fukuda, H. T. T. Nhu, O. Stelmashenko,
981 F. L. M. Peçanha, R. Rodriguez-Diaz, E. Bushong, others, Structural basis for delta cell paracrine
982 regulation in pancreatic islets. *Nature communications* **10**, 1–12 (2019).

983 59. C. Miranda, M. Begum, E. Vergari, L. J. Briant, Gap junction coupling and islet delta-cell function
984 in health and disease. *Peptides* **147**, 170704 (2022).

985 60. D. W. SCHARP, C. B. KEMP, M. J. KNIGHT, W. F. BALLINGER, P. E. LACY, The use of
986 ficoll in the preparation of viable islets of langerhans from the rat pancreas. *Transplantation* **16**, 686–
987 688 (1973).

988 61. Y. Stefan, P. Meda, M. Neufeld, L. Orci, others, Stimulation of insulin secretion reveals
989 heterogeneity of pancreatic B cells in vivo. *The Journal of clinical investigation* **80**, 175–183 (1987).

990 62. J. V. Rocheleau, M. S. Remedi, B. Granada, W. S. Head, J. C. Koster, C. G. Nichols, D. W. Piston,
991 Critical role of gap junction coupled KATP channel activity for regulated insulin secretion. *PLoS*
992 *biology* **4**, e26 (2006).

993 63. J. Zmazek, M. S. Klemen, R. Marković, J. Dolenšek, M. Marhl, A. Stožer, M. Gosak, Assessing
994 different temporal scales of calcium dynamics in networks of beta cell populations. *Frontiers in*
995 *physiology* **12**, 337 (2021).

996 64. J. D'Errico, fminsearchbnd, fminsearchcon
997 (https://www.mathworks.com/matlabcentral/fileexchange/8277-fminsearchbnd-fminsearchcon).
998 *MATLAB Central File Exchange* .

999 65. C. Y. Cha, Y. Nakamura, Y. Himeno, J. Wang, S. Fujimoto, N. Inagaki, Y. E. Earm, A. Noma,
1000 Ionic mechanisms and Ca2+ dynamics underlying the glucose response of pancreatic beta cells: a
1001 simulation study. *Journal of General Physiology* **138**, 21–37 (2011).

1002 66. A. Pisania, G. C. Weir, J. J. O'neil, A. Omer, V. Tchipashvili, J. Lei, C. K. Colton, S. Bonner-
1003 Weir, Quantitative analysis of cell composition and purity of human pancreatic islet preparations.
1004 *Laboratory investigation* **90**, 1661–1675 (2010).

67. D. B. Johnson, Efficient algorithms for shortest paths in sparse networks. *Journal of the ACM (JACM)* **24**, 1–13 (1977).

68. P. Erd\Hos, A. Rényi, On the evolution of random graphs. *Publ. Math. Inst. Hung. Acad. Sci* **5**, 17–60 (1960).

Acknowledgements
Richard KP Benninger (University of Colorado) is the guarantor of this work and, as such, had full access to all the data in the study and takes responsibility for the integrity of the data and the accuracy of the data analysis. We thank David W Piston (Washington University St Louis) with whom data presented in figure 6 was previously acquired. We thank Aaron Clauset for helpful conversations and advice. All authors acknowledge that no conflict of interest exists.

Funding:
National Institute of Health (NIH) grant R01 DK102950 (RKPB)
National Institute of Health (NIH) grant R01 DK106412 (RKPB)
National Science Foundation (NSF) Graduate Research Fellowship DGE-1938058_Briggs (JKB)
Juvenile Diabetes Research Foundation (JDRF) grant 3-PDF-2019-741-A-N (VK)
Beckman Research Institute-City of Hope (HIRN) grant 25B1104 (VK)
National Institute of Health (NIH) grant F31 DK126360 (JMD).
The authors are grateful for utilization of the SUMMIT supercomputer from the University of Colorado Boulder Research Computing Group, which is supported by the National Science Foundation (awards ACI-1532235 and ACI-1532236), the University of Colorado Boulder, and Colorado State University. Microscopy use was supported in part by NIH grant P30 DK116073 and the University of Colorado Neurotechnology center.

Author Contributions:
Conceptualization: JKB, RKPB, VK
Methodology: JKB, RKPB, VK, JMD
Investigation: JKB, VK
Visualization: JKB
Supervision: RKPB
Writing—original draft: JKB
Writing—review & editing: JKB, RKPB, VK, DJA, JMD

Competing interests: The funders had no role in the study design, data collection, and analysis, decisions to publish, or preparation of the manuscript.

Data and materials availability:
Raw microscopy imaging data to the EMBL-EBI-supported BioImage Archive. Analysis code, Model code, and Simulated Data will be available via GitHub at
https://github.com/jenniferkbriggs/Functional_and_Structural_Networks.git

Tables

Network Essentials				
Statistics			***Network Types***	
Degree	Number of edges for a given node	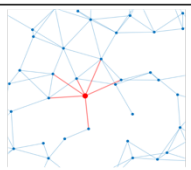	Regular	A network with ordered connections: high clustering coefficient and long average path length 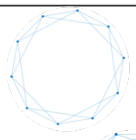
Degree Distribution	The distribution of the network's degrees		Small World	A regular network with a few rewired edges: high clustering coefficient and short average path length
Clustering Coefficient	Likelihood of how often neighbors of a node share connections with each other $\frac{3(\#\text{ of triangles})}{(\#\text{ of connected triples})}$	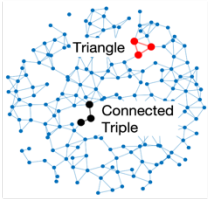	Random	A network with random connections has low clustering coefficient and short average path length
Shortest Path	Shortest distance between any two nodes	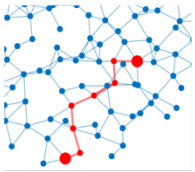	Scale-free	A network whose degree distribution follows a power law, such that there are a few very highly connected nodes called hubs
Efficiency	Inverse of the shortest path		Weighted	A network whose edges are weighted by some edge property

Table 1: Essential network statistics and types

Left: Five networks statistics used to quantify the network in this paper. Representative networks show an example of the statistic in red and the rest of the network in blue. Right: Five network types referred to in this paper. Regular, small world, and random networks are all made with the same number of nodes and edges, but different configurations of edges. Scale free network shows three "hub" nodes where node size is proportional to degree.

1056 **Figures**

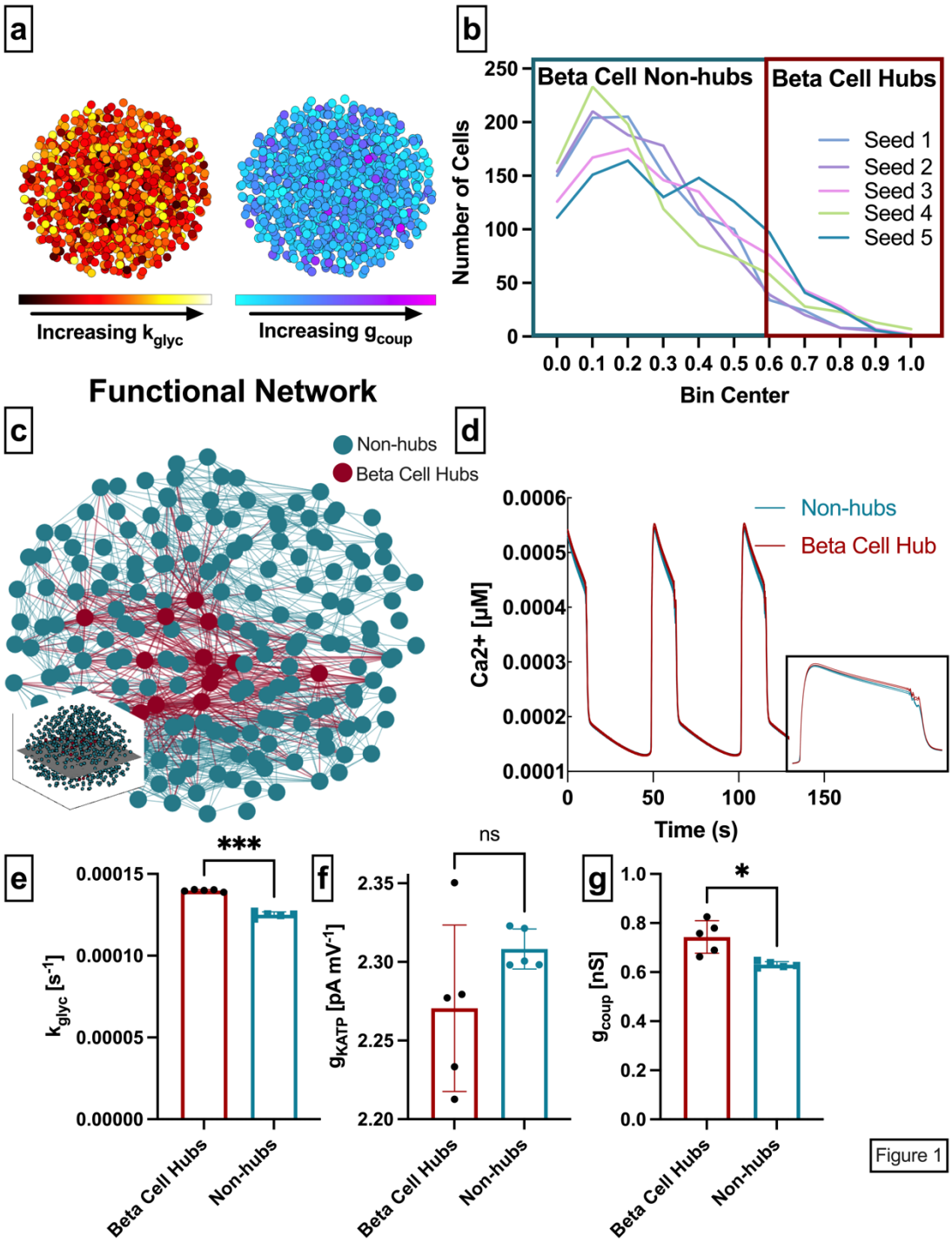

1057

1058 **Figure 1: Analysis of parameters underlying highly connected cells in a simulated islet**
1059 **network.**
1060 **a:** schematic of 1000 β-cell computational model, with cells false-colored by heterogeneity in k_{glyc}
1061 (left) and g_{coup} (right) parameter values. **b:** Distribution of functional connections (edges),

determined from functional network analysis. Colors show five seeds. Hub cells (red outline) are any cell with $> 60\%$ of maximum number of links. The R^2 for linear fit was 0.559. **c:** 2-dimensional slice of the simulated islet, with lines (edges) representing functional connections between synchronized cells. Hub cells indicated in red. Slice is taken from middle of the Islet (see inset). **d:** Representative [Ca^{2+}] time-course of a hub (red) and non-hub (blue). Inset shows zoomed enlarged signal from 45 – 80 seconds. **e:** Average rate of metabolism (k_{glyc}) parameter values compared between hub and non-hub, retrospectively analyzed. **f:** as in e for maximum conductance of ATP sensitive potassium channel (g_{KATP}). **g:** as in e for gap junction conductance (g_{coup}). Significance in e-g was determined by paired Students t-test. $*P \leq 0.05$ and $***P \leq 0.001$

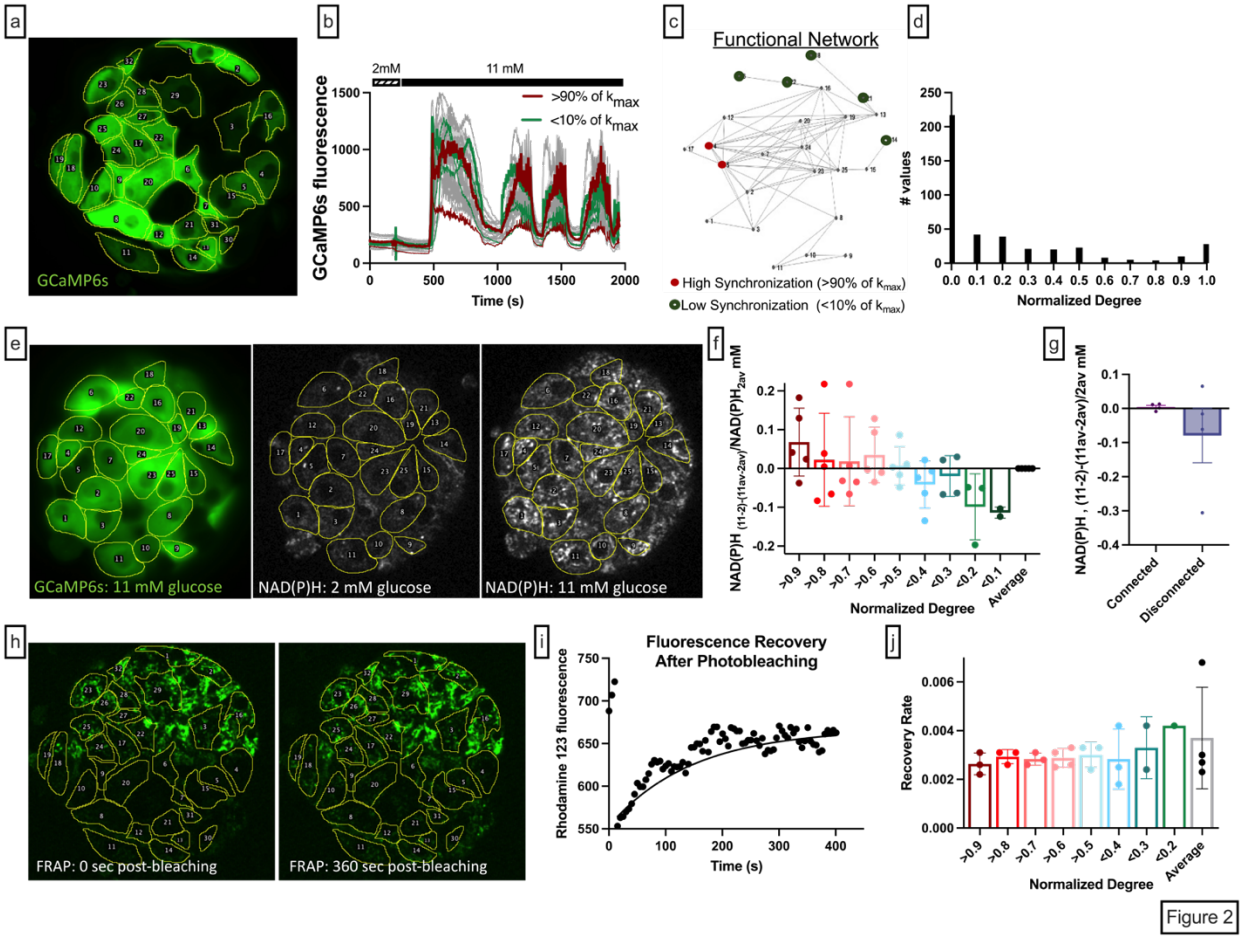

Figure 2: Comparison of the calcium-based network with the metabolic activity, NAD(P)H and coupling conductance

a: Mouse pancreatic islet expressing fluorescent calcium indicator GCaMP6s in β-cells. Glucose level 11 mM. **b:** GCamp6s time traces recorded at 2- and 11-mM glucose. Red curves represent dynamics of the most coordinated cells. These cells had highest number of edges, i.e., normalized degree >0.9. Green curves represent dynamics of the least coordinated cells, i.e., normalized degree <0.1, the rest of the cells are shown in grey. **c:** Ca^{2+} - based functional network of the islet shown in (e). Red dots represent most coordinated cells, and green dots – least coordinated cells which had at least 1 edge. **d:** Degree distribution of all eight analyzed islets. Threshold of R_{th}=0.9 was used to filter the Pearson-based coordination matrix and obtain the functional network. **e:** *Left:* Mouse pancreatic islet expressing fluorescent calcium indicator GCaMP6s. Glucose level 11 mM. *Middle:* NAD(P)H autofluorescence of the same islet and the same cell layer, recorded at 2 mM glucose. *Right*: *:* NAD(P)H autofluorescence recorded at 11 mM glucose. **f:** Change of the NAD(P)H levels in each cell in response to glucose elevation, with respect to the islet-average change. Metabolic activity here is compared for connected and disconnected cells. **g:** Change in NAD(P)H levels in response to glucose elevation, with respect to the islet-average change: here comparison is made for the most coordinated cells (normalized degree >0.9) with the less

coordinated cells (normalized degree >0.8, >0.7, >0.6, …<0.2, <0.1). f,g represent n=5 islets with a total of 131 cells. **h:** Rhodamine123 fluorescence of the same islet and the same cell layer as in ***a,*** recorded immediately after photobleaching of the bottom half of the islet **(left)** and recorded at 360 seconds after the photobleaching **(right)**. **i:** Time trace of the fluorescence recovery after photobleaching (FRAP) of the lower half of the islet, shown in **h**. The rate of recovery is proportional to the Cx36 gap junction permeability of each cell. **j:** FRAP recovery rate (sec^{-1}) in each of the photobleached cells: here the comparison is made for the most coordinated cells (normalized degree >90%) with the less coordinated cells (normalized degree >80, >70, >60, …<20, <10%). j shows results from 4 islets and 202 cells). All the cells in this graph had a degree larger than 0.01.

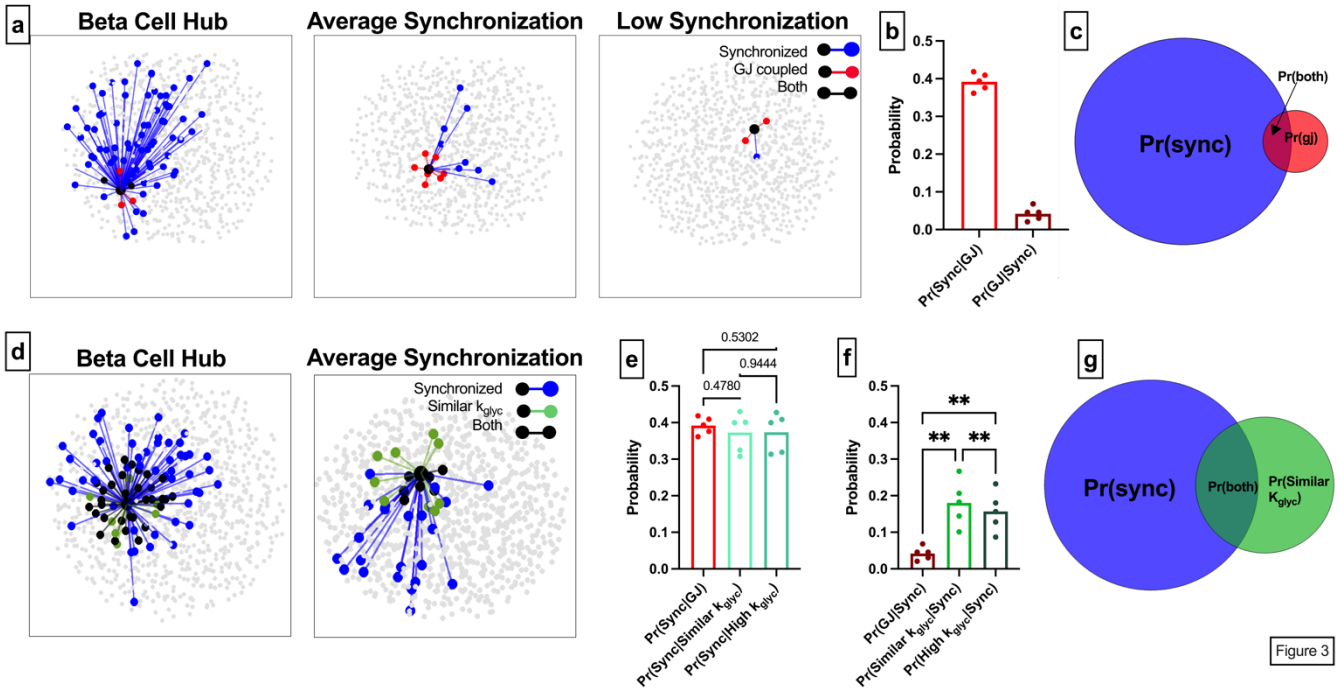

Figure 3: Comparison of functional connections, gap junction junctions, and glucose metabolism

a: Functional connections and structural connections for a representative highly connected β-cell hub, average cell, and low connected cell. Blue cells and edges indicate cells determined as "synchronized" via functional network analysis. Red cells are GJ coupled. Black cells are both GJ coupled and synchronized. **b:** Probability that a cell is synchronized given it is gap junction coupled, or vice versa, that a cell is gap junction coupled given it is synchronized. **c:** Ven diagram showing overlap between the synchronized cells and gap junction coupled cells within the simulated islet. **d:** Functional connections and metabolic connections for a β-cell hub and a cell with averaged synchronization. Blue cells and edges indicate cells determined as "synchronized" via functional network analysis. Green cells and edges indicate cells that have similar k_{glyc} and are within 15% of the islet from each other. Black cells and edges indicate both synchronized and similar k_{glyc}. **e:** Probability that a cell pair is synchronized given it shares a gap junction, has high average k_{glyc} or has similar k_{glyc}. **f:** Probability that the cell pair is gap junction coupled, has higher than average k_{glyc} and within 15% of islet distance ($Pr = 0.0050$), or has similar k_{glyc} and within 15% of islet distance ($Pr = 0.0052$), respectively, given the pair is synchronized. **g:** Ven diagram showing overlap between the synchronized cells and metabolically similar cells. Shaded area in c and g is proportional to indicated probability. Significance in e and f was determined by a repeated measures one-way ANOVA with Tukey's multiple comparisons $^{**}P \leq 0.01$.

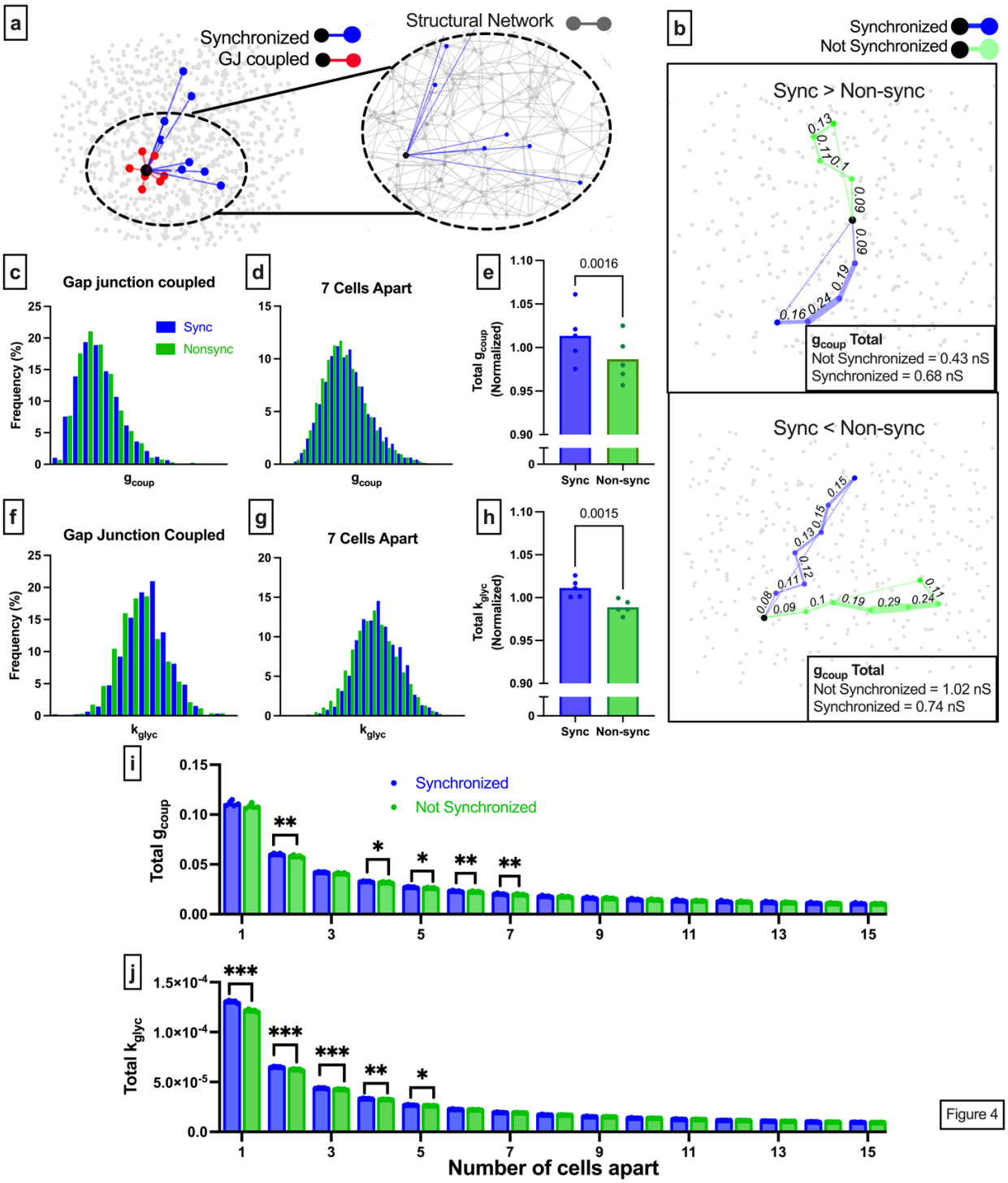

Figure 4

Figure 4: Comparison of long-range functional synchronization, gap junction network, and glucose metabolism.

a: Functional connections and gap junction connections for a representative cell (black). Synchronized cells in blue, gap junction coupled cells in red. Inset shows representative structural network (grey). **b:** Two representative cells (black) and the shortest path to a synchronized cell

(blue) and a non-synchronized cell (green). Path is weighted (shown by edge thickness) by g_{coup}. For the cell on the top panel, the synchronized path has a higher cumulative gap junction conductivity (0.68 nS) than the non synchronized path (0.43 nS). for the cell on the bottom panel, the synchronized path has a lower cumulative gap junction conductance (0.74 nS) than the non synchronized path (1.02 nS). **c:** Probability distribution of total g_{coup} for synchronized cells (blue) and non-synchronized cells (green) that are directly connected by gap junctions. **d:** As in c for cells pairs that are 7 cells apart. **e:** Comparison of the total g_{coup}, normalized by distance for synchronized cells (blue) and non-synchronized cells (green). Each dot indicates the average resistance for a single simulated islet. **f:** As in c but with connections weighted by rate of metabolism. **g:** As in d but with connections weighted by the rate of glucose metabolism. **h:** As in e but with connections weighted by the rate of glucose metabolism. **i:** Total g_{coup} for synchronized and non synchronized cells organized by cell distance. **j:** As in i but for metabolically weighted network. Significance in e,h was assessed by a two-tailed paired t-test, with P value indicated. Significance in i and j was, assessed by paired t-tests with Bonferroni correction. Reported P values are adjusted. $*P \leq 0.05$, $**P \leq 0.01$, $***P \leq 0.001$.

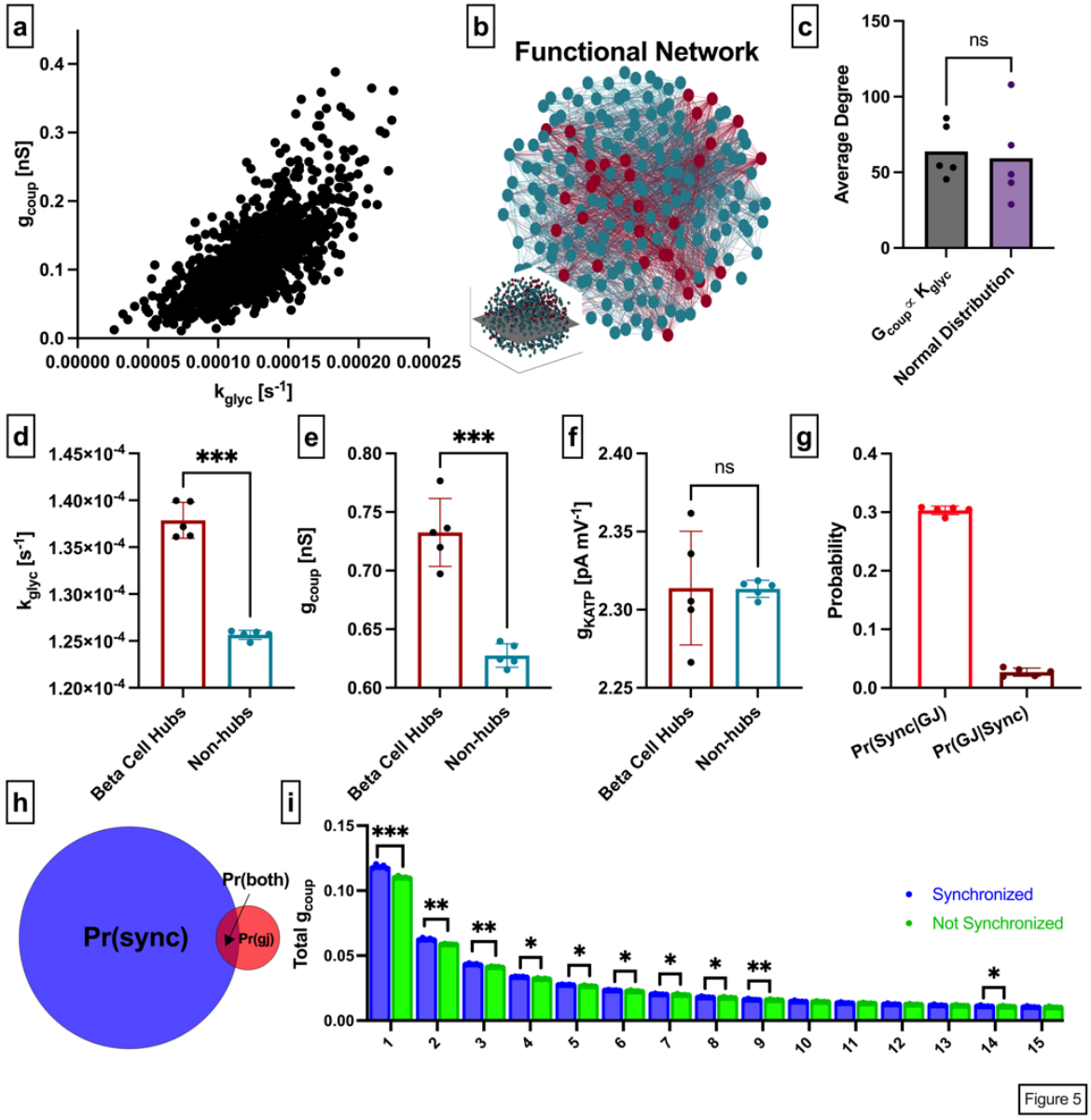

Figure 5: Assessment of functional and structural network overlap in a correlated distribution of glucose metabolism and gap junction conductance

a: Distribution where g_{coup} is correlated with k_{glyc}, such that cells with high metabolism also have high gap junction coupling. **b:** 2-dimensional slice of the simulated islet, with lines (edges) representing functional connections between synchronized cells. β-cell hubs are indicated in red. Slice is taken from middle of the Islet (see inset). **c:** Average degree comparing proportional distribution shown in a and normal distribution (Figure 1), where there is no relationship between k_{glyc} and g_{coup} **d:** Average rate of glucose metabolism (k_{glyc}) parameter values compared between hub and non-hub, retrospectively analyzed. **e:** as in d for gap junction conductance (g_{coup}). **f:** as

in d for maximum conductance of ATP sensitive potassium channel (g_{KATP}). **g:** probability of synchronization given a cell pair is gap junction coupled P(Sync|GJ), and probability that a cell pair which is gap junction coupled, is synchronized P(GJ|Sync). **h:** Venn diagram showing overlap between synchronized cell pairs and gap junction connected cell pairs. **i:** Total g_{coup} for synchronized and not synchronized cell pairs organized by cell distance. Shaded area in h is proportional to indicated probability. Significance in c-g was determined by 2-tailed paired Students t-test. Significance in i was assessed by paired t-tests with Bonferroni correction. $*P \leq 0.05$, $**P \leq 0.01$, $***P \leq 0.001$.

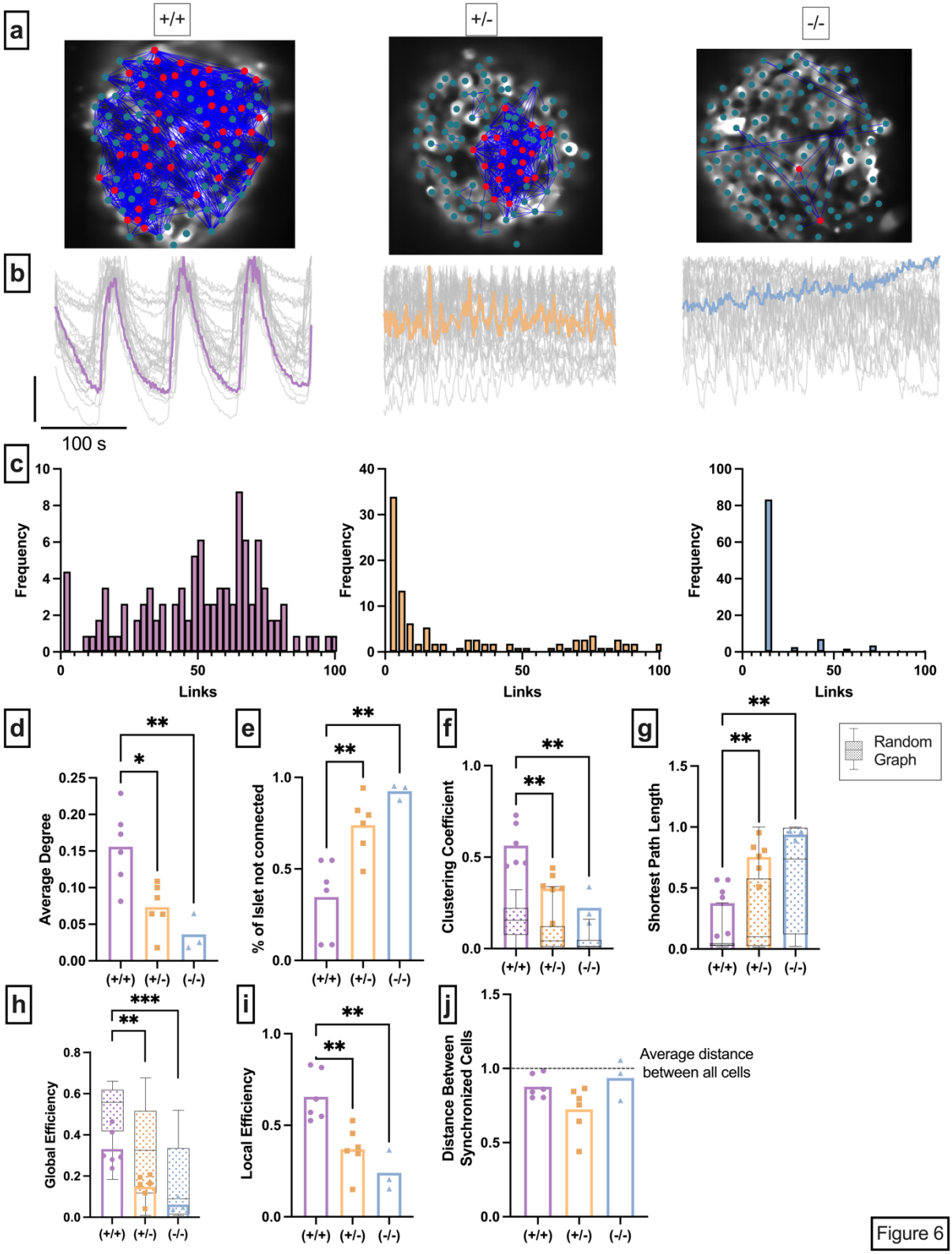

Figure 6

1163

Figure 6: Experimental islet functional network is influenced by changes in the structural network

a: Representative images of $Cx36^{+/+}$ islet (left), heterozygous $Cx36^{+/-}$ islet (middle), and homozygous $Cx36^{-/-}$ islet (right), overlaid with a synchronization network. Dot signifies a cell, blue lines represent functional network edges that connect synchronized cells. Red cells are β-cell hubs. **b:** Oscillations in $[Ca^{2+}]$ of corresponding islet in a. grey lines represent time-course for each cell, colored line represents mean islet time-course. **c:** Frequency histograms of connections for the corresponding Islet in a. Connections are calculated using functional network analysis and normalized to the maximum degree in the Islet. As such 100% links represents the cell with the greatest total number of connections. **d:** Normalized degree of functional network between cell pairs, averaged over islets of each $Cx36^{+/+}$, $Cx36^{+/-}$, $Cx36^{-/-}$ mouse. **e:** Percent of cells in the Islet which have are not connected to any other cell (eg. All $R_{ij} < R_{th}$). **f:** Average clustering coefficient. Overlaid is the box and whisker plot of 1000 random networks per Islet created with the same number of nodes, edges, and degree as the islet. **g:** Average Shortest path length. Overlaid is the box and whisker plot of 1000 random networks per islet, as in f. **h:** Average Global Efficiency. Overlaid is the box and whisker plot of 1000 random networks per islet, as in f. **i:** Local efficiency. **j:** Average number of pixels between synchronized cells normalized to the average number of pixels between all cells in the Islet. $D < 1$ indicates that cells preferentially synchronize to nearby cells. Significance in d-k determined by ordinary one-way ANOVA with Tukey multiple comparison test. Reported P values are adjusted. $*P \leq 0.05$, $**P \leq 0.01$, $***P \leq 0.001$.

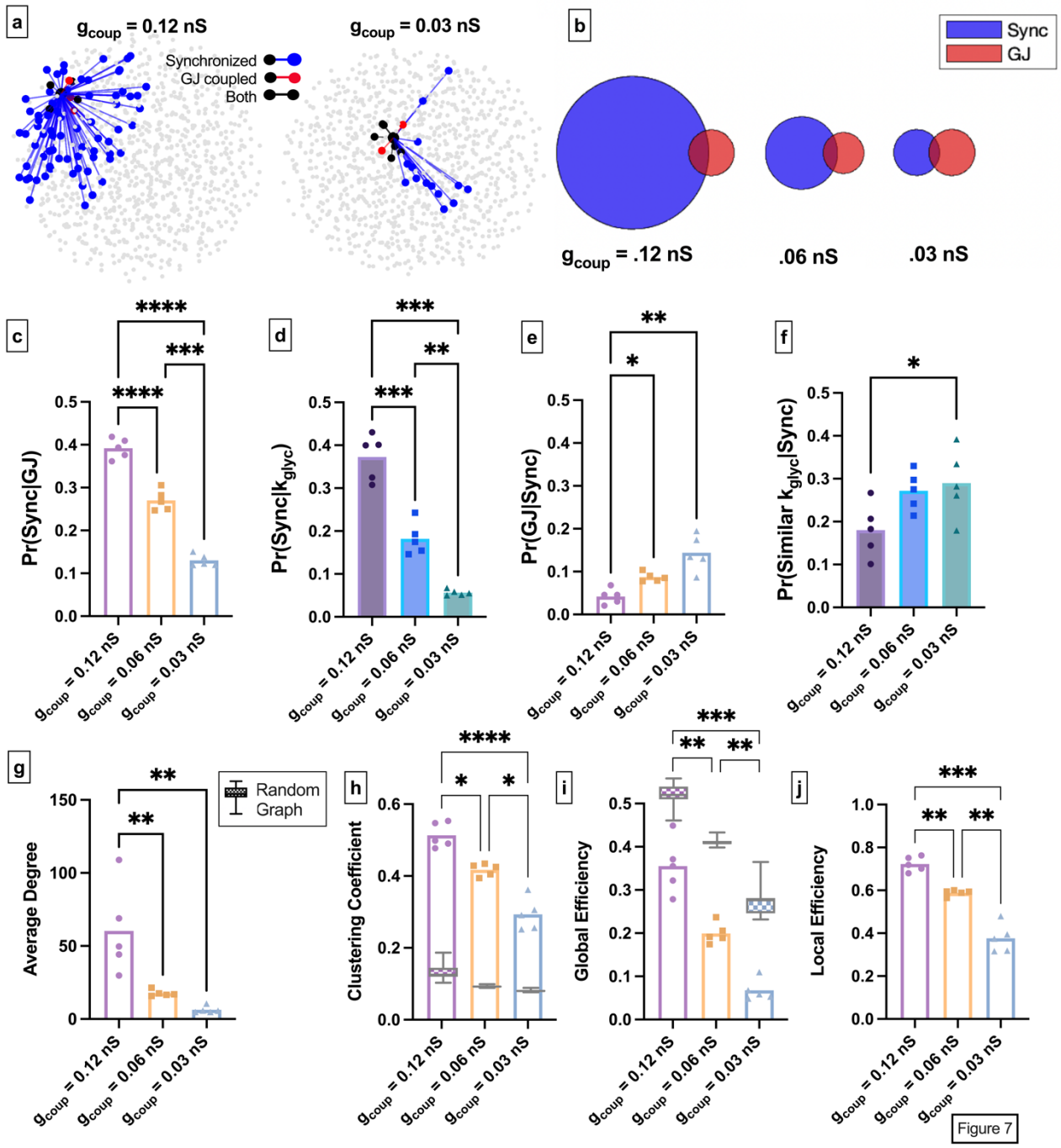

Figure 7: Simulated islet functional network is influenced by changes in the structural network

a: Representative cells within a simulated islet with high gap junction conductance ($g_{coup} = 0.12nS$) (left) and within an islet with gap junction low conductance ($g_{coup} = 0.03\ nS$)(right). Connections between a representative cell are shown with synchronized cell pairs in blue, gap junction cell pairs in red, and both in black. All data points represent the average statistic for each mouse. **b:** Venn diagrams of the probability of synchronization and probability of gap junction

with the probability of both synchronization and gap junction as the overlapped area. **c:** Probability that two cells are synchronized given they share a gap junction connection. **d:** Probability that two cells were synchronized given they had similar rate of glucose metabolism and were within 15% of the islet from each other. **e:** Probability that two cells shared a gap junction connection given they were synchronized. **f:** Probability of similar rate of glucose metabolism given two cells were synchronized. **g:** Global efficiency for $0.12nS, 0.06nS$, and $0.03nS$, for each islet seed. Overlaid is the box and whisker plot of 1000 random networks per simulated islet seed. **h:** Clustering coefficient for $0.12nS, 0.06nS$, and $0.03nS$, for each islet seed. Overlaid is the box and whisker plot of 1000 random networks per simulated islet seed, as in g. **i:** Small world-ness of a network calculated using global efficiency. 1000 random networks per islet were created to determine uncertainty of each data point (shown in black). **j:** Local efficiency for $0.12nS, 0.06nS$, and $0.03nS$, for each islet seed. Shaded area in b is proportional to indicated probability. Statistical significance in c-j assessed by an ordinary one-way ANOVA with Tukey multiple comparison test. Reported P values are adjusted. $*P \leq 0.05$, $**P \leq 0.01$, $***P \leq 0.001$.

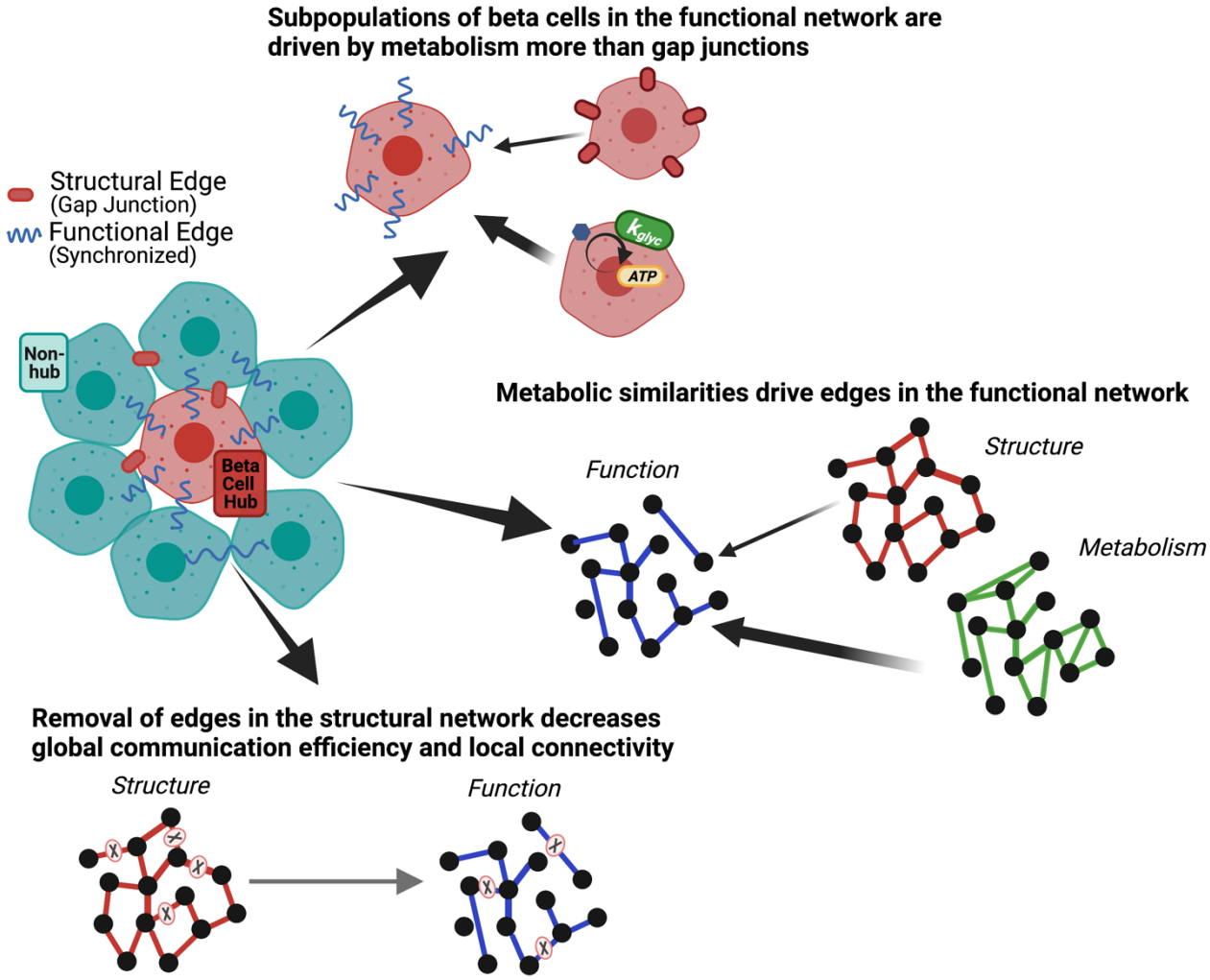

Figure 8: Graphical summary of Results

Graphical summary of results from data. To answer question 1: we show that sub populations of β-cells in the functional network are driven by metabolism more than gap junction coupling (Top). To answer question 2: we show that metabolic similarities drive edges in the functional network (right). To answer question 3: we show that removal of edges in the structural network decreased global communication efficiency and local connectivity (bottom).

SUPPLEMENTARY MATERIALS FOR

What do Functional Synchronization Networks Indicate About Underlying Structure and System Dynamics? A network theory study of the islet.

Jennifer K. Briggs, Vira Kravets, JaeAnn M. Dwulet, David J. Albers, Richard K. P. Benninger*

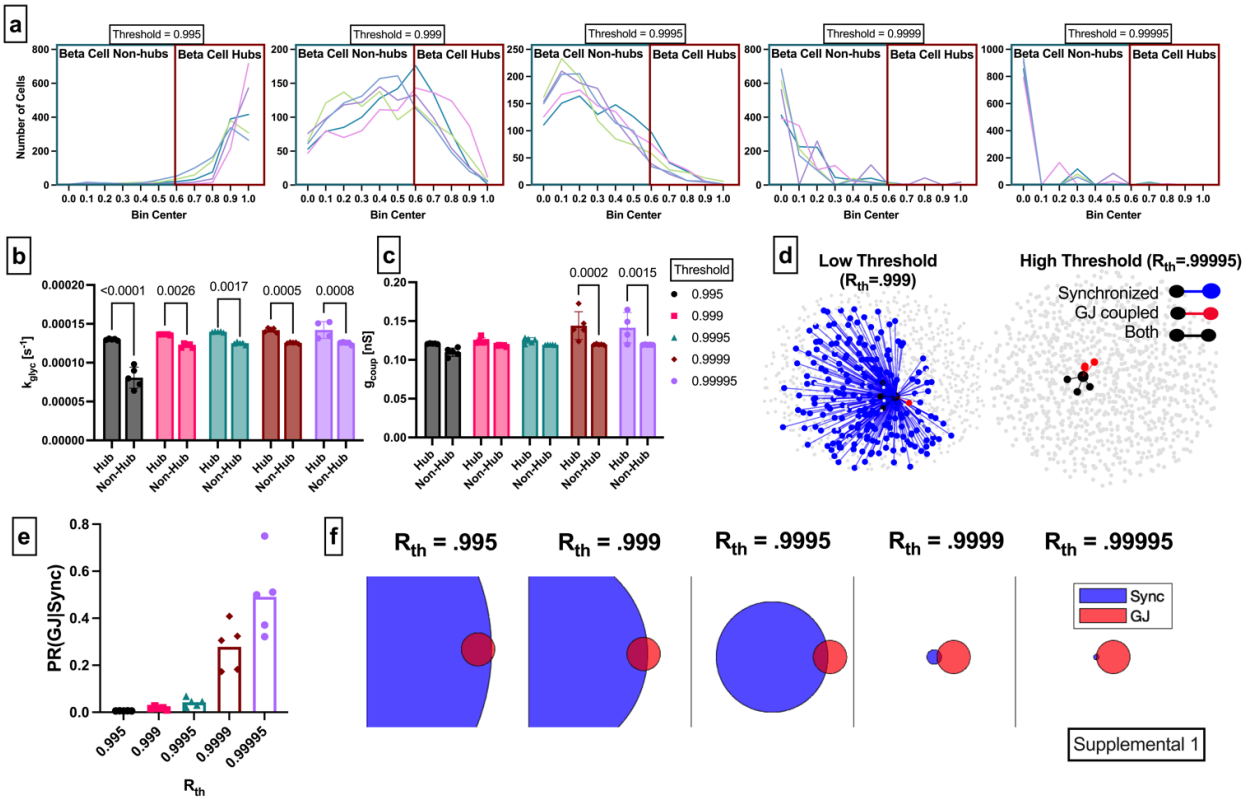

Fig. S1. Network sensitivity to threshold

a: Degree distribution of five simulated islets with five different thresholds. **b:** k_{glyc} comparing hubs and non hubs across five different thresholds. **c:** g_{coup} comparing hubs and non hubs across five different thresholds. Significance is assessed using Tukeys Multiple Comparisons. **d:** Islet with representative cell connections calculated by a lower threshold ($R_{th} = 0.999$) (**right**) and higher threshold ($R_{th} = 0.99995$) **(left)**. Synchronized cell pairs are shown in blue, gap junction pairs are shown in red and both are shown in black. **e:** Probability of a gap junction connection given synchronization for the five thresholds. **f**: Venn diagrams for the probability of synchronization (blue) and gap junction connection (red) with the overlapping area representing cell pairs that were both synchronized and gap junction coupled.

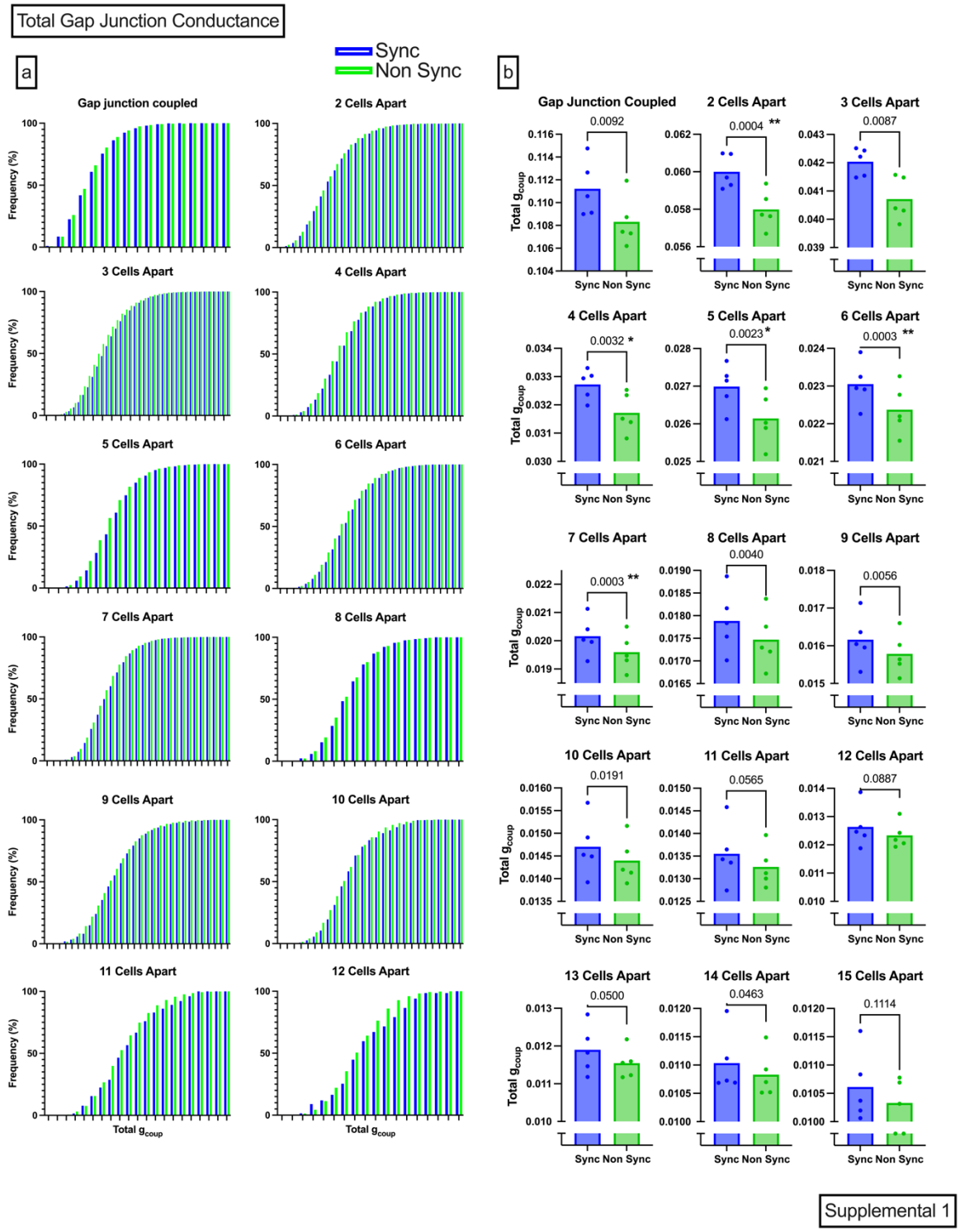

Fig. S2: Paths that maximized gap junction conductivity.

a: Cumulative distribution functions of total conductance between two cells from 1-12 cells apart. Synchronized CDF is shown in blue, non-synchronized CDF is shown in green. **b**: Bar charts comparing the average conductance for synchronized and non-synchronized cells. P values are not corrected, but

significance (denoted by asterisks) is determined using a Bonferroni-corrected paired T-test. Since we there were 15 cell distances, we set the significance threshold $\alpha = 0.003$.

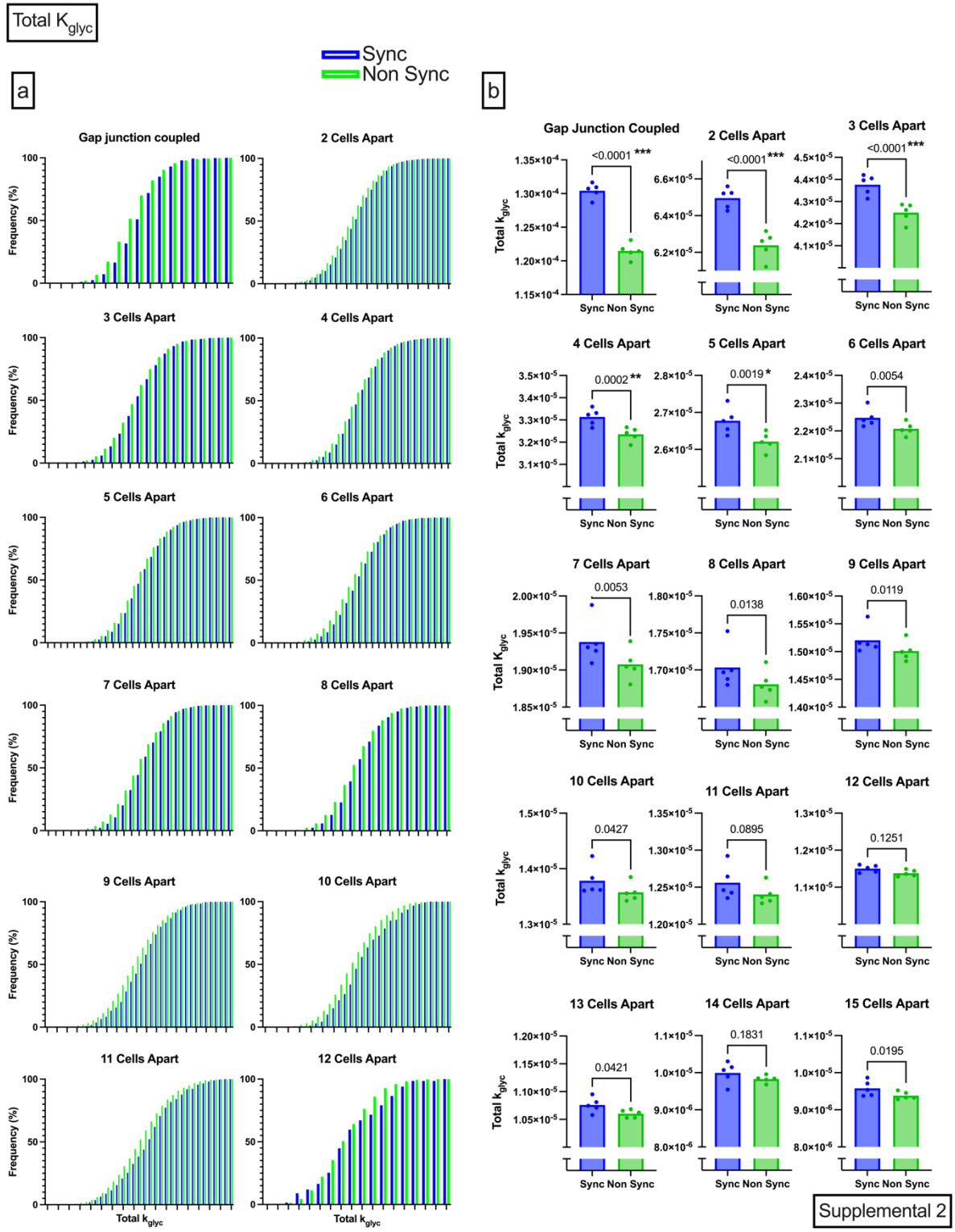

Fig. S3. Paths that maximized metabolic rate.

a: Cumulative distribution functions of total k_{glyc} between two cells from 1-12 cells apart. Synchronized CDF is shown in blue, non-synchronized CDF is shown in green. **b:** Bar charts comparing the average conductance for synchronized and non-synchronized cells. P values are not corrected, but significance

(denoted by asterisks) is determined using a Bonferroni-corrected paired T-test. Since we there were 15 cell distances, we set the significance threshold $\alpha = 0.003$.

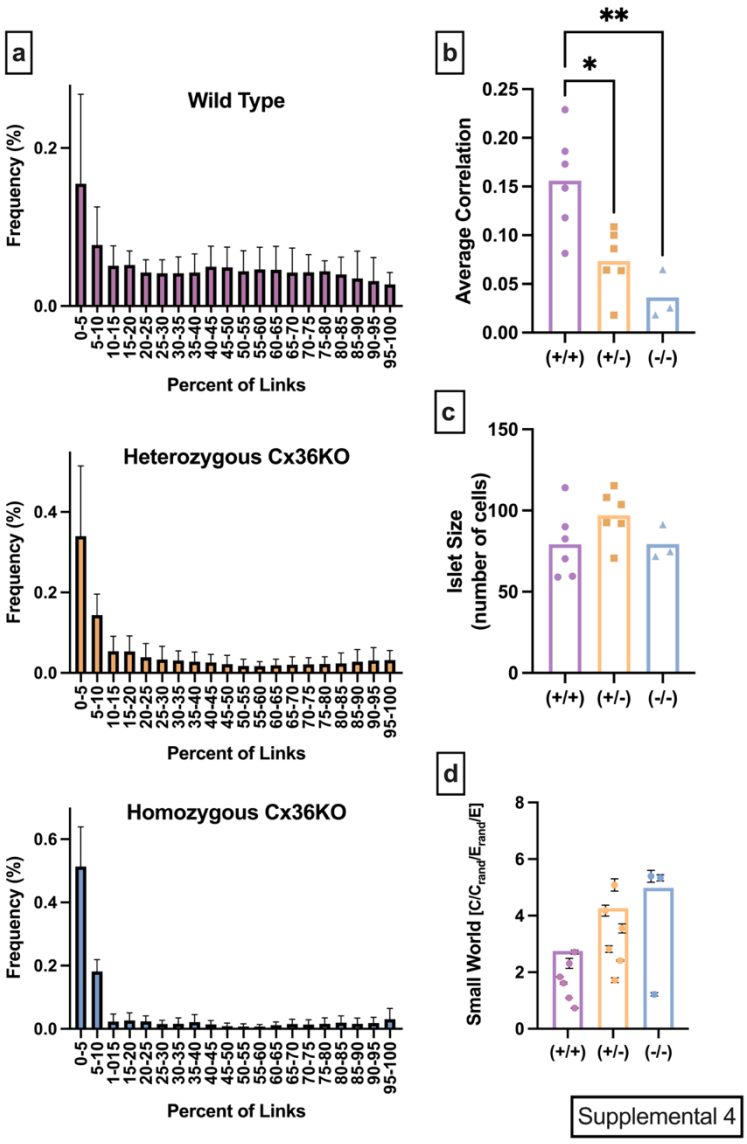

Fig. S4: Alternative Network Metrics for Calcium Islets from Cx36-KO mice

a: Averaged degree distribution histograms for all Islets analyzed. Error bars indicate standard deviation. Purple (**top**) histogram shows the distribution of connections for wild type ($Cx36^{+/+}$) islets. Orange (**middle**) shows the distribution of connections for heterozygous Cx36 knockout ($Cx36^{+/-}$) islets. Blue (**right**) shows the distribution of connections for homozygous Cx36 knockout ($Cx36^{-/-}$) islets. **b**: Average Pearson cross-correlation coefficient, between all cells in the islet. **c:** Number of cells in each islet. **d**: Small world-ness of a network calculated using global efficiency. 1000 random networks per islet were created to determine uncertainty of each data point (shown in black). Significance, or lack thereof is determined by an ordinary one-way ANOVA and Tukey Multiple comparison test. $*P \leq 0.05$, $**P \leq 0.01$

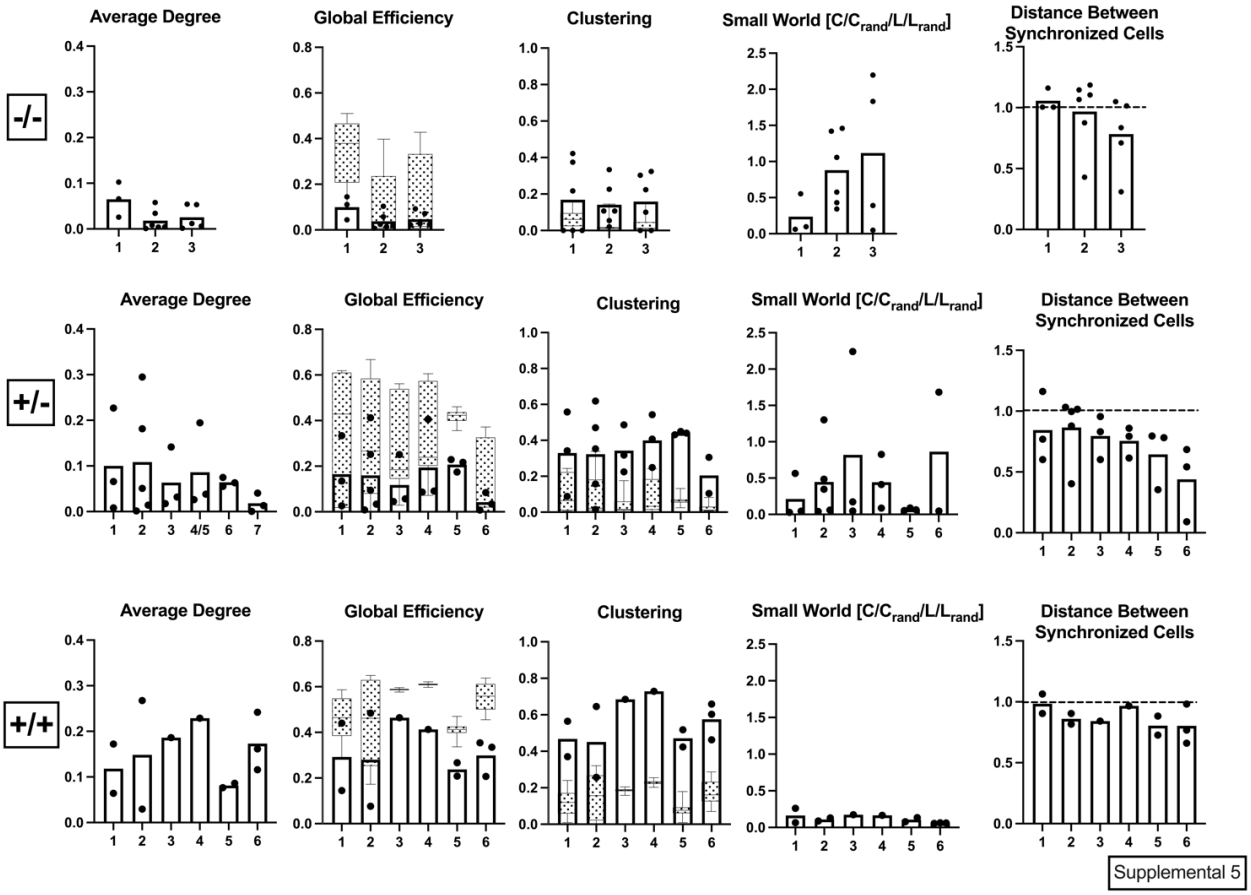

Fig. S5: Network Metrics assessed by Islets

This figure shows similar information as that of Figure 7, but the data points are individual islets and the bars are those Islets grouped by mouse. Genotypes from top to bottom: homozygous Cx36 knockout ($Cx36^{-/-}$) islets, heterozygous Cx36 knockout ($Cx36^{+/-}$) islets, wild type ($Cx36^{+/+}$) islets. Random network distributions are overlayed as box-and-whisker plots.

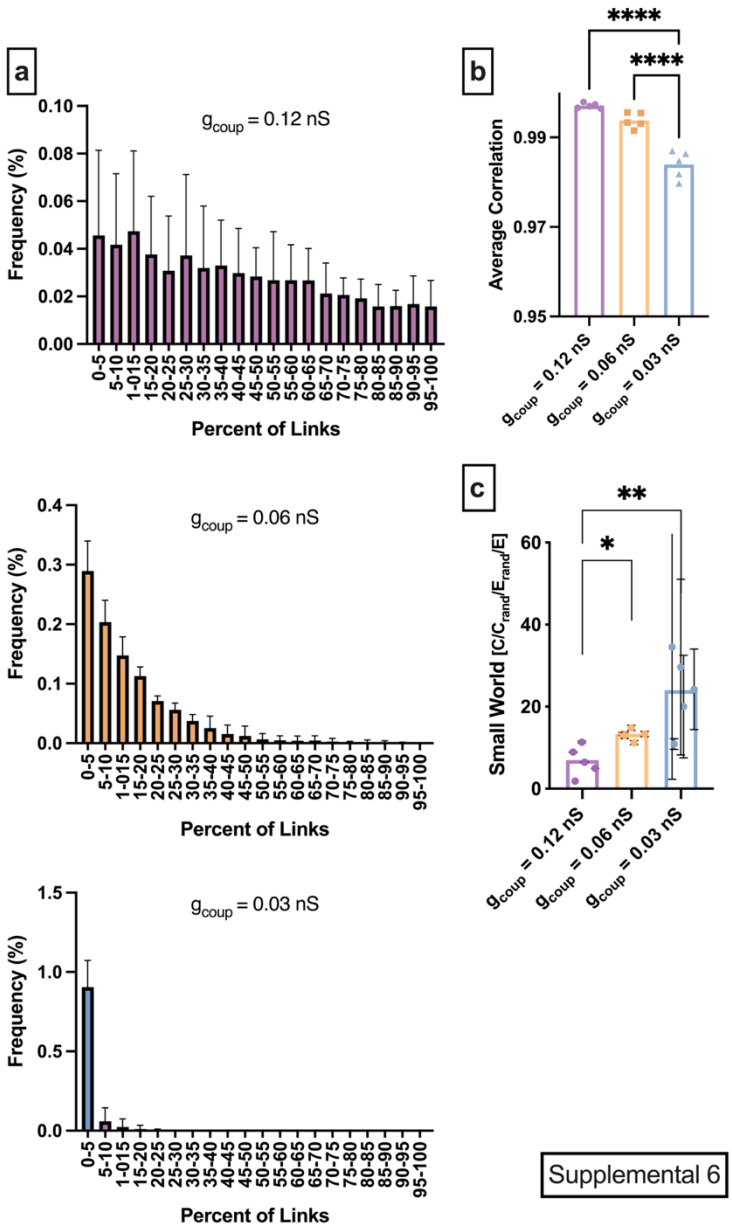

Fig. S6: Alternative Network Metrics for Simulated Islet with Gap Junction Coupling Change
a: Averaged degree distribution histograms for all Islets analyzed. Error bars indicate standard deviation. Purple (**top**) histogram shows the distribution of connections for fully coupled (0.12 nS) islets. Orange (**middle**) shows the distribution of connections for half coupled (0.06 nS) islets. Blue (**right**) shows the distribution of connections for homozygous quarter coupled (0.03 nS) islets. **b**: Average Pearson cross-correlation coefficient, between all cells in the islet. **c:** Small world-ness of a network calculated using global efficiency. 1000 random networks per islet were created to determine uncertainty of each data point (shown in black). Significance, or lack thereof is determined by an ordinary one-way ANOVA and Tukey Multiple comparison test . $*P \leq 0.05$, $**P \leq 0.01$